Participation in the Scientific Activities of the Waves in Space Plasma (WISP) Project

NASA Grant NAG5-1925

Final Report

For the period 15 March 1992 through 14 March 1994

Principal Investigators
Yakov L. Alpert (Investigation A)
Mario D. Grossi (Investigation B)

April 1994

Prepared for
National Aeronautics and Space Administration
Goddard Space Flight Center
Greenbelt, Maryland 20771

Smithsonian Institution
Astrophysical Observatory
Cambridge, Massachusetts 02138

The Smithsonian Astrophysical Observatory
is a member of the
Harvard-Smithsonian Center for Astrophysics

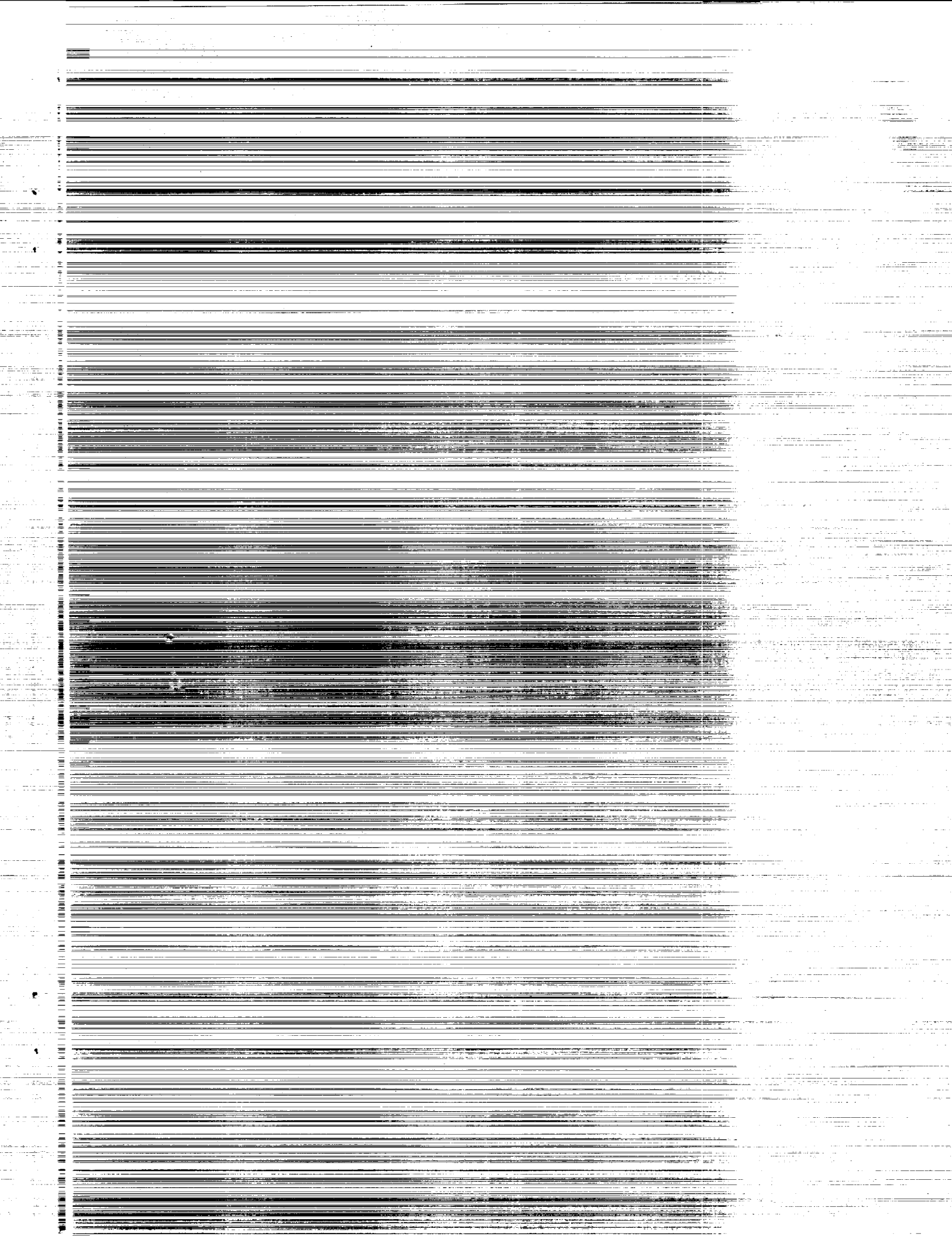

SUMMARY

This is the Final Report for Contract NAG5-1925, that consisted of experiment design, for possible use by the space science mission called WISP (Waves in Space Plasma). This mission is under study by the Canadian Space Agency and by NASA. Two WISP configurations are contemplated,under the name of BICEPS: one is called BOLAS, and the other WISPRS. Both these configurations are meant to perform bistatic sounding of the ionosphere, at a height close to F_2H_{max} (about 350 Km), with a pair of satellites, either tethered or in free flight.

INVESTIGATION A (with Y.L. Alpert as P.I.) addressed the subject of parametric decay effects, expected to arise in a magnetoplasma under the influence of high-intensity HF fields. Criteria were formulated that could be used in searching for parametric instabilities and of electric fields in the ionosphere and magnetosphere, by in-situ satellites, such as the BICEPS pair.

INVESTIGATION B (with M.D.Grossi as P.I.) addressed the bistatic measurement, by the BICEPS pair,of ionospheric features, such as large-scale and small-scale disturbances, Travelling Ionospheric Disturbances, electron density irregularities, spread-F phenomena, etc. These measurements by BICEPS could be correlated with the waveform distortion and degradation experienced by microwave links from geosynchronous height to ground, such as the ACTS satellite, expected to radiate pulses as short as 1 nanosecond in the band 20 to 30 GHz. These links are transionospheric and propagate e.m. waves in the volume of the ionosphere where BICEPS operates. It will be possible, therefore, to correlate the two classes of measurements, and learn the causative mechanisms that are resposible for the time-spread and frequency-spread nature of communications waveforms at microwave,in geosynchronous height to ground paths.

Investigation A

Longitudinal ELF to LF electromagnetic oscillations and waves generated in the ionosphere due to the non-linear parametric instability

by Yakov L. Alpert

Contents

Abstract

The essential results of this study, namely of the analytical and mainly of the detailed numerical calculations of some parametric decay effects, arising in a magnetoplasma under the influence of a HF, sufficiently strong electric field $\vec{E} = \vec{E_p} \cdot \cos \omega t$, are given in this final report. The resonance branches and the VLF parametric resonances are calculated in the ionosphere at altitudes $Z = 200, 300\,400\ km$. The values of E_p in the resonance regions were evaluated in the kinetic approximation. It is shown that the angle dependence $\omega_1(\Theta,\ E_p \neq 0)$ of the ELF $(0 < \omega \leq \Omega_B)$ resonance branch is close to the cosine law. This is in contrast with the earlier published results and with the angle dependence $\omega_1(\Theta,\ E = 0)$. This effect and the other discussed here dependencies may be used for search of parametric instabilities and of the electric field in the ionosphere and magnetosphere, especially by experiments in situ on satellites.

I. Introduction

The creation of the non-linear theory of *parametric decay effects*, produced in a magnetoplasma under the action of a high frequency electric field $E_p \cos \omega_E t$, where ω_E is much larger or comparable with the Langmuir plasma frequency ω_0, began about 30 years ago. See, for example, the papers by Silin and Aliev & Silin, 1964, 1965, 1966, [1 to 3] ; Du-Bois & Goldman, 1965, 1967 [4, 5], Nishikawa, 1967, 1968 [6, 7], and the comprehensive monograph of Silin, 1973, [8]. However, until now these phenomena were a very little studied in the free plasma surrounding the Earth, in the ionosphere and

magnetosphere. Some causes of this situation may be the following.

Such kind of experiments done in situ by satellites should be accompanied by delicate manipulations between the source of the electromagnetic field (the transmitter) and the receiver. The expected spectrum of the excited oscillations is rather various. Thus, the experimental research and the discovery of these phenomena is not a simple task. On the other hand, the general theory predicts various non-linear parametric phenomena, which should be created in the ionosphere and magnetosphere. However, to find them, particularly on satellites and for successful theoretical treatment of experimental data, the knowledge of the precise conditions of the experiment, of the basic characteristics of the magnetoplasma, of the values of E_p and ω_E, etc. is required.

To perform such experiments and to discover the parametric phenomena in the ionosphere and magnetosphere is important. It will be an essential contribution to the knowledge of the ionosphere and to the plasma physics in general. The parametric effects will be separated, divorced from many other linear and non-linear phenomena because of their special character. This will also help to understand other peculiar effects recorded in the ionosphere and magnetosphere which have not been explained until now. On the other hand, the theoretical treatment of these experiments will promote the development of the non-linear parametric theory of a magnetoplasma. Namely the noted reasons and the planned by NASA proper missions induced the theoretical calculations presented here. They are based on the general theory developed earlier (see [8]).

II. Some initial data and characteristics of the plasma

The oscillations of the electrons of a plasma under the action of an alternating sufficiently strong electric field $E_p \cos \omega_E t$ are changing essentially the electromagnetic oscillatory behavior of the media. This happens when the velocity of the oscillation of the electrons $\dot{\vec{r}}_E \parallel \vec{E}$ becomes much larger or, in some cases, only comparable with the thermal velocity v_e of the electrons when the frequency ω_E is comparable with the electron Langmuir frequency $\omega_0 = (4\pi N \cdot e^2/m)^{1/2}$. This condition which has the form

$$\dot{r}_E = \frac{e}{m}\frac{E_p}{\omega_E} \sim, \gg v_E = \left(\frac{2\kappa T_e}{m}\right)^{1/2}, \quad \omega_E \sim \omega_0 \tag{1}$$

brings to the basic inequality of the phenomena discussed here

$$\frac{E_p^2}{4\pi} \gg N\kappa T, \tag{2}$$

where T is the temperature of the plasma particles. It means that the energy density of the electric field should be much larger than the thermal energy density of the electrons, i.e. larger of their pressure. In such conditions, a new kind of instabilities and resonances, and other peculiar properties of the spectra of the excited waves and oscillations appear in the plasma. This mechanism is the so called *parametric decay instability and resonance of the plasma in the strong pump waves* $\vec{E} = E_p \cos \omega_E t$. The necessity of strong waves, i.e. of large amplitudes E_p of the electric field, and also of large frequencies of the pumped wave $\omega_E \gg, \sim \omega_0$, is directly seen from (1) and (2). However, it is shown below, that in some cases, namely in the resonance region $\omega_E \sim \omega_0$, the amplitude of the electric field may be even much smaller

than, let us say, the *characteristic* amplitude E_{p0} of the parametric non-linear effect which may be determined as

$$E_{p0} = (4\pi N \kappa T_e)^{1/2}. \tag{3}$$

Another important characteristic value which appears in the theory of the parametric non- linear effects in a plasma is the following:

$$\rho_p = \vec{k} \cdot \vec{r}_E = \frac{2\pi}{\lambda} \cdot \frac{e}{m} \frac{E_p}{\omega_E^2} = 1.91 \cdot 10^7 \cdot \frac{E_p}{\omega_E^2} \cdot \omega \cdot n(\omega). \tag{4}$$

In (4) $k = 2\pi/\lambda = \omega \cdot n/c$ is the wave number, c is the velocity of e.m. waves in free space, $n = n(\omega)$ is the index of refraction of the local region of the plasma, and λ is the wave length of the waves.

In this study we are mainly interested in the very low - VLF ($\Omega_B < \omega \leq \Omega_L$) and low - LF ($\Omega_L < \omega < \omega_B$) frequency bands. But some data are also given for the extra low ELF ($0 < \omega \leq \Omega_B$) and high frequency HF ($\omega_B < \omega \rightarrow \omega_0 ...$) bands.[1], where $\Omega_B = (e \cdot B)/(c \cdot M_{eff})$ and $\omega_B = (e \cdot B)/(c \cdot m)$ are the ion and electron angular gyro-frequencies and $\vec{B}$ is the constant magnetic field of the Earth. The ion Langmuir frequency $\omega \sim \Omega_0 = (4\pi N \cdot e^2/M_{eff})^{1/2}$ (M_{eff} is the effective mass of the ions) belongs to the LF frequency band. The results of calculations presented here were done for the ionosphere at altitudes $Z = 200$, 300, and 400 km. This region is described by the values of the parameters given in the following table, where besides the ones used above, some other characteristics of the plasma can be found. These values were used in the numerical calculations given in the next section.

[1]The classification of the frequency bands used here was introduced in [9].

Characteristics of the Ionosphere

Z, km	N, cm^{-3}	ν_{ei}, s^{-1}	T, ^oK	v_e, cm/s	$\frac{M_{eff}}{M_{H1}}$	v_i, cm/s	ω_0, Hz
200	$5.0 \cdot 10^5$	$2.0 \cdot 10^3$	1000	$1.1 \cdot 10^7$	12	$7.4 \cdot 10^4$	$4.0 \cdot 10^7$
300	$1.8 \cdot 10^6$	$3.0 \cdot 10^3$	1500	$2.0 \cdot 10^7$	5	$2.1 \cdot 10^5$	$7.6 \cdot 10^7$
400	$1.5 \cdot 10^6$	$1.5 \cdot 10^3$	1800	$2.8 \cdot 10^7$	3	$3.8 \cdot 10^5$	$6.9 \cdot 10^7$

Z, km	Ω_0, Hz	Ω_L, Hz	Ω_B, Hz	ω_B, Hz	n_A	V_A, m/s	ρ_e, cm
200	$2.7 \cdot 10^5$	$5.3 \cdot 10^4$	364	$8.1 \cdot 10^6$	742	$4.04 \cdot 10^5$	1.35
300	$7.9 \cdot 10^5$	$7.9 \cdot 10^4$	834	$7.7 \cdot 10^6$	947	$3.16 \cdot 10^5$	2.60
400	$9.3 \cdot 10^5$	$9.8 \cdot 10^4$	1327	$7.3 \cdot 10^6$	701	$4.28 \cdot 10^5$	3.83

Z, km	ρ_i, cm	$4\pi N\kappa T_e$, erg/cm^3	E_{p0}, $CGSE$	E_{p0}, V/m	D_e, cm	D_e^2, cm^2
200	203	$8.67 \cdot 10^{-7}$	$9.31 \cdot 10^{-4}$	27.9	0.198	$3.78 \cdot 10^{-2}$
300	252	$4.68 \cdot 10^{-6}$	$2.16 \cdot 10^{-3}$	64.9	0.186	$3.46 \cdot 10^{-2}$
400	286	$4.68 \cdot 10^{-6}$	$2.16 \cdot 10^{-3}$	64.9	0.286	$8.21 \cdot 10^{-2}$

In addition to the notations given above, in this table E_{p0} is the characteristic amplitude of the electric field (see (3)), D_e is the Debye length of the electrons, $D_e^2 = \kappa T/4\pi Ne^2$, the ions effective mass

$$M_{eff} = M_{H_1} \cdot \sum_s \frac{N_{is}}{N_i} \cdot \frac{M_{H_1}}{M_{is}}, \tag{5}$$

N_{is}, M_{is} are, respectively, the densities and masses of the ion constituents of the plasma, $v_i = \sqrt{2\kappa T/M_{eff}}$ is the thermal velocity of the ions, the subscript H_1 is the notation of the protons, ω_L is the low-hybrid frequency, $\rho_i = v_i/\Omega_B$, ρ_e/ω_B are the ion and electron Larmor radii, $\Omega_0 = (4\pi N_e^2/M_{eff})^{1/2}$ is the

ion Lengmuir frequency, Ω_B and ω_B are the circular gyro-frequencies of the ions and electrons, $V_A = c/n_A$ and $n_A = \Omega_0/\Omega_B$ are the velocity and index of refraction of the Alfven waves.

We consider here a quasi-neutral $N_e = N_i$ and isothermal $T_e = T_i$ plasma, i.e. that the energy densities and the Debye lengths of the electrons and ions are equal,

$$N_e \kappa T_e \sim N_i \kappa T_i, \quad kD_e \sim kD_i. \tag{6}$$

III. Theoretical equations, formulas, results of numerical calculations

The following theoretical results in this section give a qualitative and an approximate quantitatively representation of the behavior of the e.m. plasma oscillations and waves, excited parametrically in the ionosphere under the action of the electric field $E_p \cdot \cos \omega_E t$.

The equations used here are based on different asymptotic solutions of the dispersion equation. For example, to calculate the resonance branches, the cold plasma approximation was mostly used. I.e. the values $\omega_i = k \cdot v_i$ and $\omega_D = k \cdot D_e$, which appear in the kinetic approximation, due to the influence of the temperature of the particles, are absent in the formulas. Nevertheless, in the ELF and VLF frequency bands these values become comparable with the frequencies of the parametric waves and they should, and were, taken into account (see below). The cold plasma approximation

can be also used by calculation of the frequencies and growth rates of the waves in the VLF resonance region. However, the amplitudes E_p of the electric field can be, and were, evaluated by the kinetic approximation. In some cases, the isotropic plasma approximation was used. I.e. the influence of the constant magnetic field was not completely taken into account, and this may be warranted since $\omega_0 \gg \omega_B$.

III-1. Resonance branches of the ionosphere

The dispersion equation of a magnetoplasma, not taking into account the thermal velocities of the electrons and ions, i.e. in the cold plasma approximation, can be conveniently represented as the following:

$$\begin{aligned} D(\omega,\Theta) &= \omega^4(\omega_B^2-\omega^2)(\Omega_B^2-\omega^2)+\omega^4\left(\Omega_0^2(\omega_B^2-\omega^2)+\omega_0^2(\Omega_B^2-\omega^2)\right)\sin^2\Theta - \\ &- \omega^2(\omega_0^2+\Omega_0^2)(\omega_B^2-\omega^2)(\Omega_B^2-\omega^2)\cos^2\Theta + \\ &+ \Omega_0^2\omega_0^2\left(1-J_0^2(\rho_p)\right)\cdot(\omega_B^2\cos^2\Theta-\omega^2)(\Omega_B^2\cos^2\Theta-\omega^2)=0, \end{aligned} \tag{7}$$

when $\omega_E \gg \omega_0$, $\omega_E \gg \omega_B$, and

$$\frac{2\pi\rho_i}{\lambda_\perp},\ \frac{2\pi\rho_e}{\lambda_\perp} \ll 1,\ \frac{v_i}{v_{\Phi\|}} \ll \left|1-s\frac{\Omega_B}{\omega}\right|,\ \frac{v_e}{v_{\Phi\|}} \ll \left|1-s\frac{\omega_B}{\omega}\right|, \tag{8}$$

where $s = 0, \pm1, \pm2, ..,$ ρ_e, ρ_i, and ρ_p were defined above,

$$v_{\Phi\|} = \frac{c}{n_\|},\ \ \lambda_\perp = \frac{2\pi c}{n_\perp\omega} = 2\pi\frac{v_{\Phi\perp}}{\omega}, \tag{9}$$

and $v_{\Phi\|}$, $v_{\Phi\perp}$ are the longitudinal and transverse phase velocities of the waves with frequency ω, and $n_\|$ and $n_\perp$ are their longitudinal and transverse in-

dexes of refraction (see [8]).

The properties of the roots of the equation $D(\omega, \Theta) = 0$ are directly visible. It estimates four wave branches $\omega_s^2(\Theta)$, $s = 1$ *to* 4. Only one of them, let us denote it $\omega_2(\Theta)$, is of pure electric field origin (see (11) and (12)). The influence of the electric field on the other resonance branches becomes clear only by analyzing the results of numerical calculations of the angle dependencies of $\omega_s(\Theta)$, where Θ is the angle between the wave vector $\vec{k}$ and the constant magnetic field $\vec{B}$ of the Earth.

When $\Theta = 0$, the frequencies $\omega_s(\Theta)$ are the following:

$$\omega_1^2 = \Omega_B^2, \quad \omega_3^2 = \omega_B^2, \tag{10}$$

$$\omega_{2,4}^2 = \frac{1}{2}\left((\omega_0^2 + \Omega_0^2) \mp \sqrt{(\omega_0^2 + \Omega_0^2)^2 - 4\omega_0^2\Omega_p^2}\right), \ \omega_2^2 \simeq \Omega_p^2, \ \omega_4^2 \simeq \omega_U^2, \tag{11}$$

where

$$\Omega_p^2 = \Omega_0^2\left(1 - J_0^2(\rho_p)\right), \quad \rho_p = \frac{e}{m}\frac{E_p}{\omega_E^2} \cdot \frac{2\pi}{\lambda}. \tag{12}$$

When $\Theta = \pi/2$,

$$\omega_1^2 = \omega_2^2 = 0, \quad \omega_{3,4}^2 = \frac{1}{2}\left((\omega_U^*)^2 \mp \sqrt{(\omega_U^*)^4 - 4\left(\omega_0^2(\Omega_p^2 + \Omega_L^2 + \Omega_B^2) + \Omega_L^4\right)}\right) \tag{13}$$

With a high accuracy

$$\omega_3^2 = \Omega_{Lp}^2 \simeq \frac{\Omega_L^2 + \Omega_p^2}{1 + \frac{\omega_B^2}{\omega_0^2}}, \ \omega_4^2 \simeq (\omega_U^*)^2 - \frac{\Omega_p^2 + \Omega_L^2}{1 + \frac{\omega_B^2}{\omega_0^2}}, \tag{14}$$

where

$$(\omega_U^*)^2 = (\omega_0^2 + \omega_B^2 + \Omega_0^2 + \Omega_B^2) \simeq \omega_U^2, \tag{15}$$

and $\Omega_L = \sqrt{\omega_B \Omega_B}$, $\omega_U = \sqrt{\omega_0^2 + \omega_B^2}$ are the generally used definitions of the Low-hybrid and High-hybrid frequencies (see also (17), (18)).

In the absence of the eclectic field, i.e when $E_p = 0$, $J^2(\rho_p) = 1$, and $\omega_2(\Theta) = 0$ the three resonance branches are the following:

$$\begin{aligned} \Theta = 0 \quad &, \quad \omega_1^2 = \Omega_B^2, \quad \omega_3^2 = \omega_B^2, \quad \omega_4^2 = (\omega_0^2 + \Omega_0^2) \simeq \omega_0^2, \\ \Theta = \frac{\pi}{2} \quad &, \quad \omega_1^2 = 0, \quad \omega_3^2 \simeq \frac{\omega_B \Omega_B}{1 + \frac{\omega_B^2}{\omega_0^2}} = \frac{\Omega_L^2}{1 + \frac{\omega_B^2}{\omega_0^2}} = (\Omega_L^*)^2 \\ & \omega_4^2 = (\omega_0^2 + \omega_B^2 + \Omega_0^2 + \Omega_B^2) - (\Omega_L^*)^2 \simeq \omega_U^2 \end{aligned} \tag{16}$$

By analyzing the angle dependencies of the dispersion equation $D(\omega, \Theta)$, it is seen that the inequalities $\omega_1(\Theta) < \Omega_B$ and $\omega_3(\Theta) < \omega_B$ should be fulfilled for all the angles $0 < \Theta < \pi/2$. However, in [8] the branch $\omega_1(\Theta)$ given on Fig.6 has a maximum at $\Theta \sim (60 - 70)^\circ$, which is comparable with Ω_p! What is the source of this maximum and of its extremely large value in comparison with Ω_B is not clear.

Actually, the numerical calculations of the resonance branch $\omega_1(\Theta)$ is a delicate job because the region of the values of different roots of $D(\omega, \Theta) = 0$ is very large. For example, in our case the values of $\omega_1(\Theta) \sim ...10^2$ are about 10^5 times smaller than $\omega_4(\Theta) \sim ...10^7$. Therefore, only by very precise numerical calculations this branch can be calculated correctly. As a result, we did find that the function $\omega_1(\Theta)$ is very *closely proportional to* $\cos\Theta$ and differs from it only in the fourth and following decimal digits. For example, at $Z = 300\ km$

$$\Omega_B \cdot \cos(0.1\pi) = 793.466\underline{451} \text{ but } \omega_1(0.1,\pi) = 793.466\underline{349},$$
$$\Omega_B \cdot \cos(0.45\pi) = 130.513\underline{274} \text{ but } \omega_1(0.45,\pi) = 130.513\underline{102},$$

and

$$D(\omega_1(0.1\pi)) > 0 \text{ by } \omega_1 = 793.466349600\underline{835},$$
$$D(\omega_1(0.1\pi)) < 0 \text{ by } \omega_1 = 793.466349600\underline{836}.$$

When $E \neq 0$, the angle dependence of the branch $\omega_1(\Theta)$ differs also very much both qualitatively and quantitatively from the dependence $\omega_1(\Theta) = \Omega_B \to 0$, when $E = 0$. This is seen from Table I and Figs.1, 2.

To find the branch $\omega_1(\Theta)$ close to the cosine rule, when $E \neq 0$, the numerical calculations were done with digits up to the (20-40), and higher order. Detailed calculations were also made to track the sharp transition of $\omega_1(\Theta) \to 0$, when $E_p = 0$.

The dependencies of all the resonance branches $\omega_{1\ to\ 4}(\Theta)$ of the ionosphere for $Z = 300\ km$, $E \neq 0$, $E_p = 0$, and $\rho_p = 1$ and also for comparison, the branch $\omega_2(\Theta)$ for $\rho_p = 0.1$ are given in Table I and Figs.1 and 2. To check the revealed here closely proportionality of the branch $\omega_1(\Theta,\ E \neq 0)$ to $\cos\Theta$ shown on Table I adn Figs.1,2, the calculations were also done by the shortened equation (7). Namely, when $\omega^2 \ll \omega_B^2$ and $\cos^2\Theta \gg m/M$, it becomes equal to:

$$D(\omega,\Theta) = \omega^4\omega_0^2(\omega_L^2 - \omega^2)\sin^2\Theta - \omega^2\omega_B^2(\Omega_B^2 - \omega^2)(\omega_0^2\cos^2\Theta - \omega^2) +$$
$$+\Omega_0^2\omega_0^2\omega_B^2(\Omega_B^2\cos^2\Theta - \omega^2)\left[1 - J_0^2(\rho_p)\right]\cdot\cos^2\Theta = 0,$$

Table I. Resonance branches, $E =, \neq 0$, $Z = 300km$,
$\omega_0 = 7.569 \cdot 10^7 Hz$, $\omega_B = 7.66 \cdot 10^6$, $\Omega_0 = 7.9 \cdot 10^5$, $\Omega_p = 5.0857996 \cdot 10^5$,
$\Omega_B = 834.3$, $E = 0$: $\omega_3 = 7.5694123 \cdot 10^7$, $\omega_U = 7.6080677 \cdot 10^7$, $\rho_p = 1$

β	Θ^o	$E=0$ ω_1, Hz	$E\neq 0$ ω_1, Hz	$E\neq 0$ ω_2, Hz	$E=0$ ω_3, Hz	$E\neq 0$ ω_3, Hz	$E\neq 0$ ω_4, Hz
0	0	Ω_B	Ω_B	Ω_p	ω_B	ω_B	$7.5692414 \cdot 10^7$
0.05	9	834.299	824.028	$5.08579 \cdot 10^5$	$7.564746 \cdot 10^6$	$7.564741 \cdot 10^6$	$7.5701994 \cdot 10^7$
0.1	18	-	793.47	-	-	-	-
0.15	27	834.288	743.37	5.08575	6.817977	6.817917	7.5772905
0.2	36	-	674.96	-	-	-	-
0.25	45	834.255	589.94	5.08563	5.402849	5.402727	7.5886940
0.3	54	-	490.39	-	4.487833	-	-
0.35	63	834.125	378.76	5.08516	3.464215	3.463922	7.6000121
0.4	72	833.870	257.81	-	2.357389	-	-
0.45	81	832.495	130.51	5.07792	1.119493	1.194196	7.6069651
0.46	82.8	831.467	104.56	5.07171	$9.58504 \cdot 10^5$	$9.57904 \cdot 10^5$	-
0.48	86.4	823.052	52.38	4.60609	4.85080	5.28379	7.6077490
0.49	88.2	791.778	26.20	2.37225	2.52242	-	-
0.492	88.56	770.529	20.97	1.89945	2.07369	5.12793	7.6078754
0.495	89.10	694.912	13.10	1.18810	1.43718	-	-
0.499	89.82	240.466	2.62	$2.3772 \cdot 10^4$	$8.3068 \cdot 10^4$	5.12217	7.6078991
0.4992	89.856	195.315	2.09	1.9017	8.1816	-	-
0.4995	89.91	124.165	1.31	1.1886	8.0439	5.12212	7.6078994
0.4999	89.982	25.101	0.26	$2.377 \cdot 10^3$	7.9579	-	-
0.49992	89.9856	20.083	0.21	1.901	7.9566	5.12210	7.6078995
0.49995	89.991	12.554	0.13	1.188	7.9522	-	-
0.49999	89.9982	2.51	0.026	$2.377 \cdot 10^2$	7.9544	5.12210	7.6078995
0.5	90	0	0	0	$\Omega_L =$	$\omega_{Lp} =$	$\omega_U =$
		10^{-28}	10^{-135}	10^{-8}	$7.9543 \cdot 10^4$	$5.12210 \cdot 10^5$	$7.6078995 \cdot 10^7$

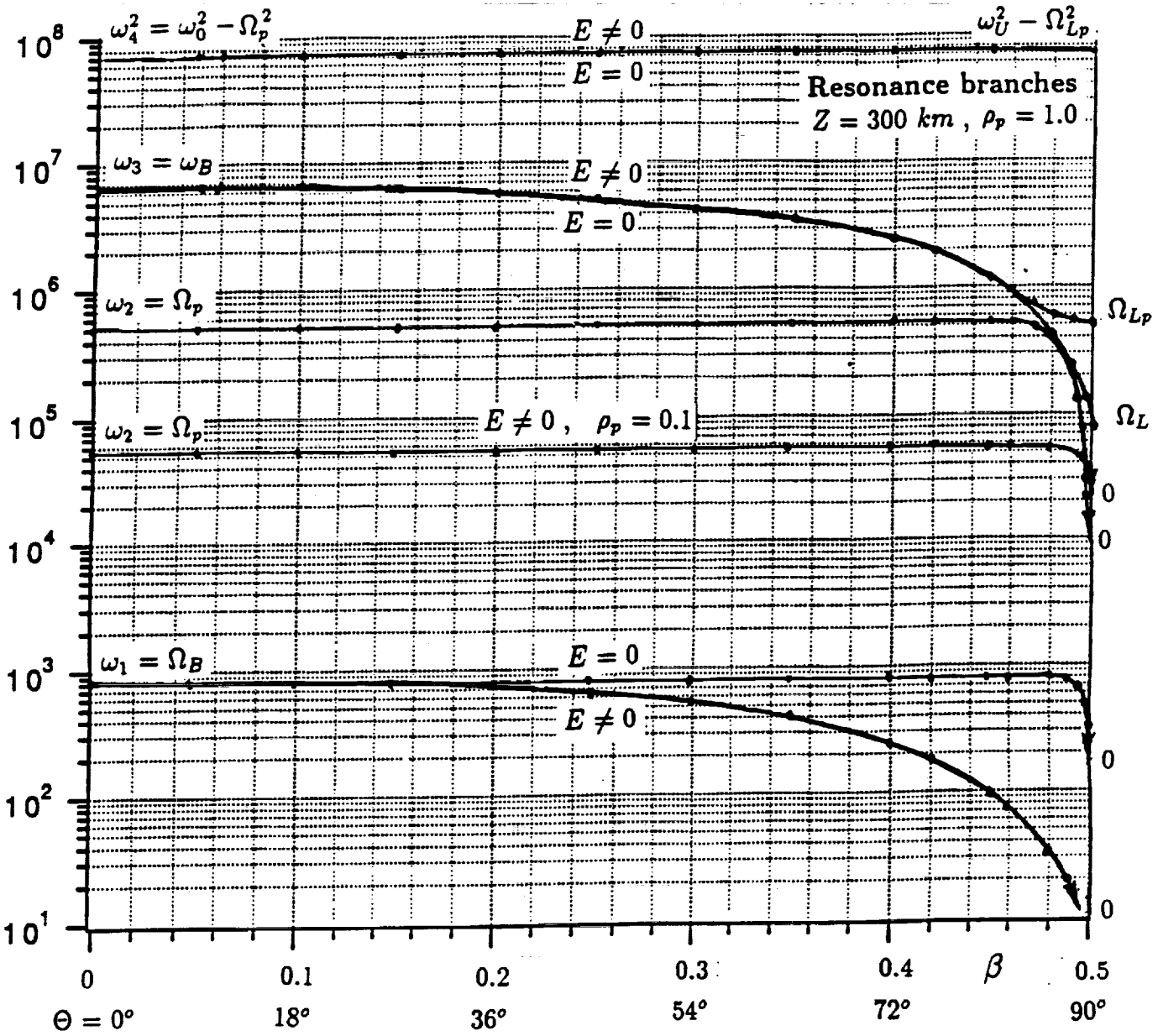

Fig 1. Resonance branches of the ionospheric magnetoplasma under the action of an alternating electric field $\vec{E} = \vec{E}_p \cdot \cos \omega_E t$, $\rho_p \sim E/\omega_E^2$ (see (4)), Θ is the angle between $\vec{E}$ and the constant Earth's magnetic field $\vec{B}$.

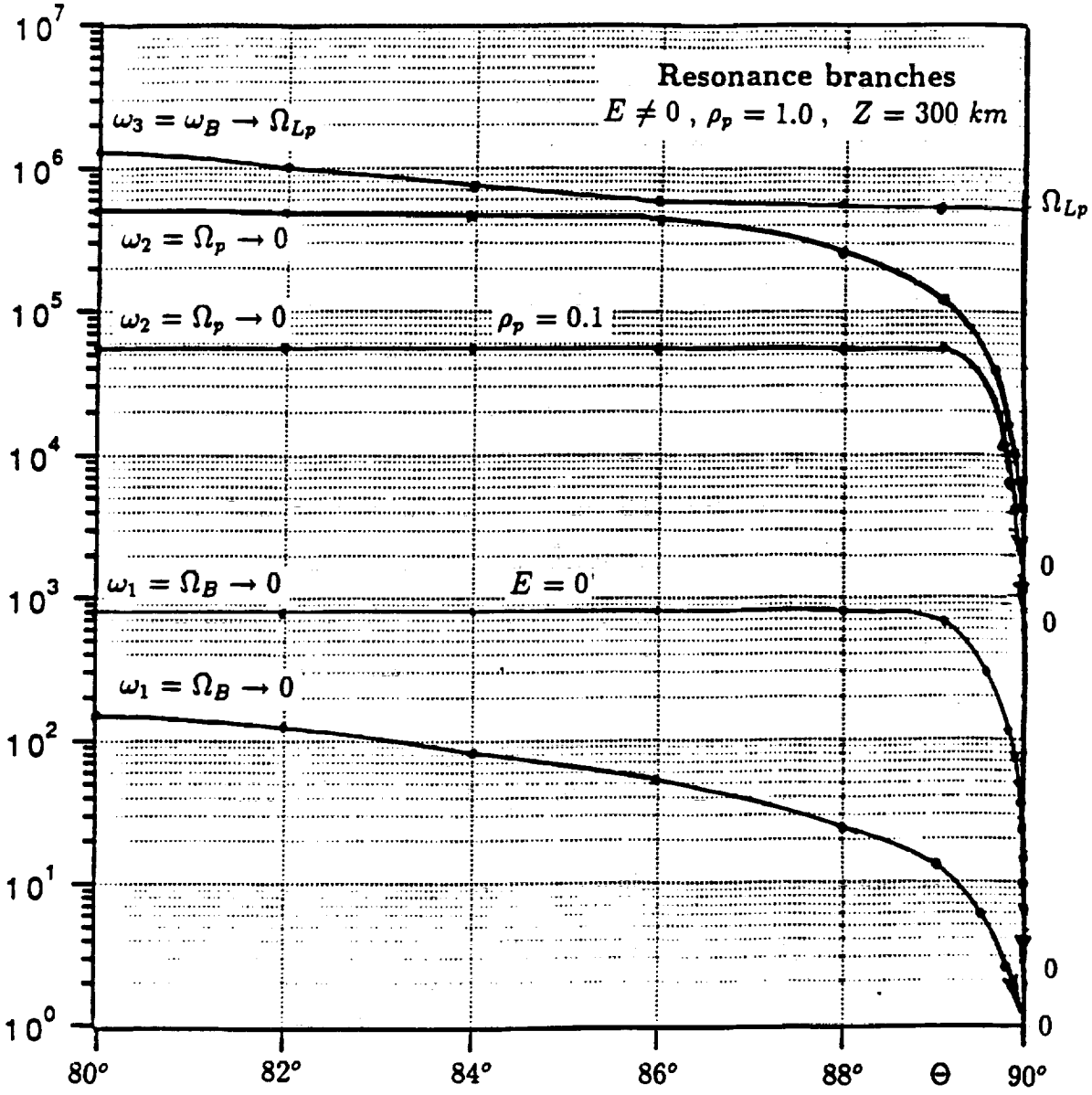

Fig 2. The same as on Fig.1 for angle range $\Theta = (80 - 90)°$.

and the numerical calculations of $\omega_1(\Theta)$ become much simpler. The results of all these calculations are in a perfect agreement. The value $\rho_p = 1$ may be considered as a strong field characteristic.

It follows from the figures and the table that the influence of the electric field is only large on the dependencies $\omega_1(\Theta)$ and $\omega_2(\Theta)$. Quantitatively, the behavior of $\omega_3(\Theta,\ E \neq 0)$ differs from $\omega_3(\Theta,\ E = 0)$ only when $\Theta \geq 80^o$ to $\sim 90^o$, namely $\omega_3(\pi/2,\ E \neq 0) = \Omega_{Lp} \simeq 5.12 \cdot 10^5\ Hz$, and $\omega_3(\pi/2,\ E = 0) = \Omega_L \simeq 7.95 \cdot 10^4\ Hz$. The influence of the electric field on the high frequency branch $\omega_4(\Theta) \simeq (\omega_0^2 \rightarrow \omega_U^2)$ is even much smaller. The so called hybrid frequency branches $\omega_3(\Theta)$ and $\omega_4(\Theta)$ are also only a few under the influence of the ions. Therefore, they can be calculated by the following simple equation

$$\omega_{3,4} \simeq \frac{1}{2}\left((\omega_0^2 + \omega_B^2) \pm \sqrt{(\omega_0^2 + \omega_B^2)^2 - 4\omega_0^2\omega_B^2\cos^2\Theta}\right), \qquad (17)$$

which is true for $\omega_3(\Theta)$ only when $\cos^2\Theta \gg m/M$. By $\Theta = \pi/2$

$$\omega_3^2 = \frac{\Omega_B\omega_B + \Omega_0^2[1 - J_0^2(\rho_p)] + \Omega_B^2 + \frac{\Omega_B^2\omega_B^2}{\omega_0^2}}{1 + \frac{\omega_B^2}{\omega_0^2}} \simeq \frac{\Omega_L^2 + \Omega_p^2 + \frac{\Omega_L^4}{\omega_0^2}}{1 + \frac{\omega_B^2}{\omega_0^2}} = \Omega_{Lp}^2 \qquad (18)$$

(see (14)).

What is of a special interest is to find in the experiments the branch $\omega_2^2(\Theta)$, which is of purely electric field origin. Depending on ρ_p, the value $\omega_2(\rho_p)$ is varying from Ω_p to 0. By small values of E_p or large frequencies ω_E, when $\rho_p << 1$, and $J_0^2(\rho_p) \sim (1 - \rho_p^2/2)$, even ELF parametric waves

$\omega_2(\Theta)$ may be excited. Therefore, by theoretical calculations of $\omega_2(\Theta)$, the thermal velocity of the particles should be taken into account, and the kinetic approximation should be used. It brings to the following equations:

$$\omega_2^2 = \cos^2\Theta \cdot \left(\frac{\Omega_0^2[1 - J_0^2(\rho_p)]}{1 + n_A^2 \cdot \sin^2\Theta \cdot [1 - J_0^2(\rho_p)]} + 3k^2 v_i^2 \right), \qquad (19)$$

and the Landau damping of these waves is equal to

$$\gamma = \sqrt{\frac{\pi}{8}} \cdot \frac{\omega^4}{|k_{||}|^3} \cdot \left\{ \frac{1}{v_i^2} \cdot Exp\left(-\frac{\omega^2}{2k^2 v_e^2} \right) + \cos^2\Theta \cdot \frac{\Omega_0^2 \omega_0^2 J_0^2(\rho_p)}{\omega^4 v_e^3} \right\}, \qquad (20)$$

when $k_\perp \rho_{ei} \ll 1$ (see the Table on p.4), $v_i \ll v_{\Phi||} \ll v_e$, taking also into account that $D_i k_i$, $D_e k_e \ll 1$. By $\rho_p \gg 1$, even when $\rho_p \sim 1$,

$$\omega^2 \simeq \frac{\Omega_0^2 \cos^2\Theta}{1 + n_A^2 \sin^2\Theta} + 3k^2 v_i^2 \cos^2\Theta. \qquad (21)$$

When $\rho_p \ll 1$ and $\Theta = 0$ (isotropic plasma),

$$\omega_2^2 = \Omega_p^2 = \Omega_0^2 \left(1 - J_0^2(\rho_p)\right) + (kv_i)^2 \simeq \frac{1}{2} \left(\frac{e}{m} \cdot \frac{\Omega_0}{\omega_p^2} \right)^2 \cdot (\vec{k} \cdot \vec{E}_p)^2 + 3(kv_i)^2. \quad (22)$$

This equation, rewritten as

$$\Omega_p^2 = 3k^2(V_p^2 + v_i^2), \quad V_p = \frac{1}{\sqrt{2}} \cdot \frac{e\Omega_0}{m\omega_p^2} E_p, \qquad (23)$$

demonstrates a very important physical result. Longitudinal ELF waves, propagating along the direction of the electric field E_p, can be parametrically excited in a plasma. Their velocity V_p is determined by (23). To find experimentally this branch of *ELF parametric waves* in the ionosphere, it would also be a great achievement of any satellite mission.

Results of calculations of the resonance branches $\omega_2(\Theta)$ and $\omega_3(\Theta)$ at different altitudes Z of the ionosphere and different values of $\rho_p \sim E_p/\omega_E^2$ are given in the Tables II and IIa. The characteristic frequencies $\omega_2(\Theta = 0) = \Omega_p$ and $\omega_3(\Theta = \pi/2) = \Omega_{Lp}$ of these branches are of pure electric field origin, they are given in the following table:

Z, km	$\rho_p = 0.1$		$\rho_p = 0.5$	
	Ω_p	Ω_{Lp}	Ω_p	Ω_{Lp}
200	$1.89 \cdot 10^4$	$5.60 \cdot 10^4$	$9.25 \cdot 10^4$	$1.05 \cdot 10^5$
300	$5.58 \cdot 10^4$	$9.70 \cdot 10^4$	$2.73 \cdot 10^5$	$2.83 \cdot 10^5$
400	$6.58 \cdot 10^4$	$1.18 \cdot 10^5$	$3.21 \cdot 10^5$	$3.34 \cdot 10^5$

Z, km	$\rho_p = 1.0$		$\rho_p = 1.5$	
	Ω_p	Ω_{Lp}	Ω_p	Ω_{Lp}
200	$1.72 \cdot 10^5$	$1.77 \cdot 10^5$	$2.30 \cdot 10^5$	$2.31 \cdot 10^5$
300	$5.08 \cdot 10^5$	$5.12 \cdot 10^5$	$6.79 \cdot 10^5$	$6.80 \cdot 10^5$
400	$5.99 \cdot 10^5$	$6.04 \cdot 10^5$	$8.00 \cdot 10^5$	$8.04 \cdot 10^5$

To illustrate the dependence of $\omega_2(\Theta = 0)$ on ρ_p (see (22)), the ratio of Ω_p/Ω_0 is also given in the following Table IIb and on Fig.2a.

Table II. Resonance branches, $E \neq 0$, $\Theta^\circ = \pi\beta$

β	Z, km	ω_2, Hz $\rho_p = 0.1$	Hz 0.5	Hz 1.0	Hz 1.5	ω_3, Hz $\rho_p = 0.1$	Hz 0.5	Hz 1.0	Hz 1.5
0	200	$\Omega_p =$ $1.8938 \cdot 10^4$	$\Omega_p =$ $9.2532 \cdot 10^4$	$\Omega_p =$ $1.72534 \cdot 10^5$	$\Omega_p =$ $2.30238 \cdot 10^5$	$\omega_B =$ $8.02 \cdot 10^6$	$\omega_B =$ $8.02 \cdot 10^6$	$\omega_B =$ $8.02 \cdot 10^6$	$\omega_B =$ $8.02 \cdot 10^6$
	300	5.5823	$2.7276 \cdot 10^5$	5.08580	6.78683	$7.66 \cdot 10^6$	$7.66 \cdot 10^6$	$7.66 \cdot 10^6$	$7.66 \cdot 10^6$
	400	6.5784	3.21429	5.99339	7.99807	7.31	7.31	7.31	7.31
0.10	200	1.8938	9.2533	1.72534	2.30239	7.61226	7.61226	7.61225	7.61225
	300	5.5824	2.72757	5.08578	6.78681	7.28154	7.28154	7.28152	7.28151
	400	6.5785	3.21427	5.99336	7.99805	6.94854	6.94853	6.94851	6.94849
0.20	200	1.8939	9.2532	1.72533	2.30238	6.44237	6.44236	6.44234	6.44321
	300	5.5824	2.72751	5.08571	6.78677	6.18624	6.18622	6.18617	6.18611
	400	6.5786	3.21416	5.99323	7.99798	5.90271	5.90268	5.90260	5.90250
0.30	200	1.8940	9.2530	1.72530	2.30236	4.65226	4.65224	4.65218	4.65212
	300	5.5822	2.72733	5.08549	6.78664	4.48783	4.48778	4.48764	4.48749
	400	6.5782	3.21382	5.99278	7.99770	4.28173	4.28165	4.28144	4.28120
0.40	200	1.8937	9.25160	1.72515	2.30226	2.43457	2.43452	2.43436	2.43419
	300	5.5800	2.72633	5.08419	6.78583	2.35738	2.35572	2.35692	2.35652
	400	6.5740	3.21183	5.99016	7.99602	2.24980	2.24929	2.24877	2.24813
0.42	200	1.8935	9.2505	1.72499	2.30218	1.95830	1.95822	1.95803	1.95781
	300	5.5783	2.72566	5.08316	6.78515	1.89743	1.89728	1.89686	1.89634
	400	6.5707	3.21030	5.98798	7.99450	1.81093	1.81071	1.81008	1.80926
0.44	200	1.8939	9.24830	1.72471	2.30200	1.47519	1.47509	1.47483	1.47453
	300	5.5746	2.72386	5.08071	6.78340	1.43042	1.43025	1.42973	1.42902
	400	6.5634	3.20686	5.98258	7.99012	1.36580	1.36558	1.36488	1.36377

Table IIa. Resonance branches, $E \neq 0$, $\Theta^o = \pi\beta$ (Continuation)

β	Z, km	ω_2, Hz $\rho_p = 0.1$	Hz 0.5	Hz 1.0	Hz 1.5	ω_3, Hz $\rho_p = 0.1$	Hz 0.5	Hz 1.0	Hz 1.5
1.46	200	$1.8915 \cdot 10^4$	$9.2418 \cdot 10^5$	$1.72387 \cdot 10^5$	$2.30148 \cdot 10^5$	$9.87130 \cdot 10^5$	$9.86981 \cdot 10^5$	$9.86584 \cdot 10^5$	9.86129 ·
	300	5.5640	2.71870	5.07171	6.77465	9.58499	9.58369	9.57904	9.5696
	400	6.5477	3.19611	5.95882	7.94867	9.16349	9.16371	9.16468	9.1684
0.48	200	1.8835	9.2056	1.72883	2.29801	4.96534	4.96299	4.95610	4.9467
	300	5.5070	2.6806	4.60609	4.76855	4.85135	4.86919	5.28379	6.8108
	400	6.4317	3.10017	4.48584	4.55145	4.66967	4.73267	6.09864	8.0212
0.49	200	1.8523	9.0454	1.68376	2.23096	2.52561	2.52652	2.53076	2.5488
	300	5.2863	2.17906	2.37225	2.38895	2.52816	2.99643	5.13210	6.8007
	400	6.0151	2.13298	2.26287	2.27853	2.49773	3.44098	6.04777	8.0151
0.499	200	$7.706 \cdot 10^3$	$2.1634 \cdot 10^4$	$2.4037 \cdot 10^4$	$2.4351 \cdot 10^4$	$6.0712 \cdot 10^4$	1.05652	1.77297	2.3183
	300	$1.3501 \cdot 10^4$	2.3087	2.3772	2.3899	9.4008	2.82860	5.12217	6.7995
	400	1.2593	2.1953	2.266	2.266	$1.19324 \cdot 10^5$	3.34378	6.04016	6.0401
0.4995	200	$4.090 \cdot 10^3$	1.0869	1.2023	1.2266	$5.7192 \cdot 10^4$	1.05140	1.77228	2.3182
	300	6.854	1.1545	1.1886	1.195	9.7510	2.82807	5.12215	6.7990
	400	6.357	1.0978	1.1330	1.1330	$1.18174 \cdot 10^5$	3.34334	6.04011	
0.4999	200	$8.35 \cdot 10^2$	$2.177 \cdot 10^3$	$2.405 \cdot 10^3$	$2.453 \cdot 10^3$	$5.6041 \cdot 10^4$	1.04983	1.77207	2.3182
	300	$1.377 \cdot 10^3$	2.309	2.377	2.390	9.7034	2.82790	5.12210	6.7990
	400	1.275	2.196	2.266	2.266	$1.17808 \cdot 10^5$	3.34320	6.04010	6.0401
0.5	200	0	0	0	0	$\Omega_{Lp} =$ $5.5993 \cdot 10^4$	$\Omega_{Lp} =$ 1.04977	$\Omega_{Lp} =$ 1.77206	$\Omega_{Lp} =$ 2.3182
	300					9.7014	2.82789	5.12210	6.7990
	400					$1.17793 \cdot 10^5$	3.34319	6.04009	6.0401

Table IIb. Frequencies of the longitudinal component ($\Theta = 0$) of the parametric resonance branch $\omega_2(\Theta)$

$$\frac{\Omega_p}{\Omega_0} = \frac{\omega_2(\Theta=0)}{\Omega_0} = \left[1 - J_0^2(\rho_p)\right]^{1/2}, \quad \rho_p = \frac{2\pi}{\lambda}\cdot\frac{e}{m}\cdot\frac{E_p}{\omega_E^2}, \quad \overline{E} = \overline{E}_p \cos\omega_E(t), \quad \omega_E \gg \omega_0$$

ρ_p	0	0.02	0.05	0.1	0.5	1.0	1.5	2.0
$J_0(\rho_p)$	1	0.9999	0.9994	0.9975	0.9385	0.7652	0.5118	0.2138
Ω_p/Ω_0	0	0.01	0.024	0.071	0.345	0.647	0.834	0.976
ρ_p	2.4048	3	3.832	5.0	5.520	6.0	6.5	7.016
$J_0(\rho_p)$	1.0	-0.2601	-0.4028	-0.1776	0	0.1506	0.2601	0.3001
Ω_p/Ω_0	max 1.0	0.966	min 0.915	0.984	max 1.0	0.988	0.965	min 0.954
ρ_p	7.5	8.0	8.5	8.650	9.0	9.5	10.0	10.713
$J_0(\rho_p)$	0.2663	0.1717	0.0419	0	-0.0903	-0.1939	-0.2459	- 0.2497
Ω_p/Ω_0	0.964	0.985	0.999	max 1.0	0.996	0.981	0.970	min 0.966

III-2. Parametric VLF resonance instabilities and oscillations.

The principal properties of the parametric resonance instabilities are, more or less, similar in an isotropic ($\vec{B} = 0$), and anisotropic ($\vec{B} \neq 0$) plasma. In an isotropic plasma the resonance regions of the parametric effects are of a special interest when $\omega_E \sim s\omega_0$, $s = 1, 2, ..$, i.e. when the frequency of the electric field is comparable with the electron Langmuir frequency or its

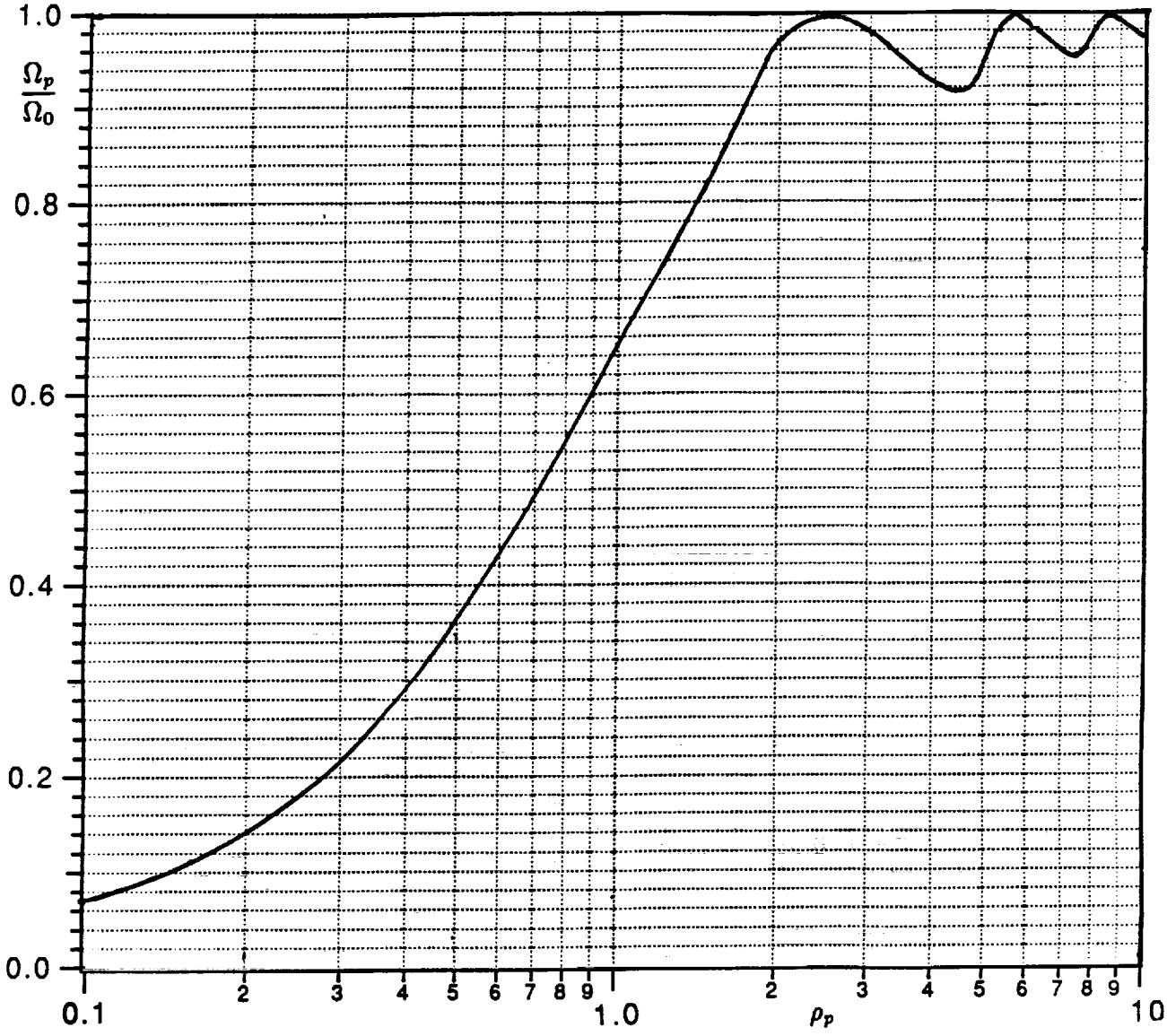

Fig 2a. Dependence of Ω_p/Ω_0 of the longitudinal component of $\omega_2(\Theta = 0) = \Omega_p$ on ρ_p.

harmonics. In an anisotropic plasma, distinguish resonance instabilities arise when the overtones of the electric field

$$s\omega_E \simeq \omega_3(\Theta), \ \simeq \omega_4(\Theta), \ \simeq [\omega_3(\Theta) + \omega_4(\Theta)], \tag{24}$$

i.e. by approaching of the resonance hybrid frequencies (see (17), (18)) or of their sum. However, the calculations of the resonances in a magnetoplasma are considerable more complicated. And for the ionosphere detailed numerical calculations are given here only when $\omega_E \simeq s\omega_0$, i.e. not taking into account the influence of the magnetic field. These results give a general qualitative and, in a sense, also a quantitative presentation of the behavior of the parametric resonance instabilities. Some equations of these instabilities in a magnetoplasma are discussed for illustration at the end of this section.

a. Isotropic plasma ($\vec{B} = 0$). The high frequency spectrum of the discussed here parametric oscillations has no peculiarities. When the frequency of the electric field is not much larger than the electron Langmuir frequency ω_0, we can approximately use for the calculation of the spectrum of this branch of oscillations the equation

$$\omega = \omega_0 \left(1 + \frac{1}{2} \sum_{s=-\infty}^{\infty} J_s(\rho_p) \cdot \frac{\Omega_0^2}{(s\omega_E + \omega_0)^2}\right). \tag{25}$$

It becomes

$$\omega^2 = \omega_0^2 + J_0^2(\rho_p) \cdot \Omega_0^2, \tag{26}$$

when $\omega_E^2 \gg \omega_0^2$.

However, the low frequency band $\omega \ll \omega_0$ of these oscillations becomes of resonance nature

$$\omega^2 = \Omega_0^2 \sum_{-\infty}^{\infty} J_s^2(\rho_p) \cdot \frac{(\omega + s\omega_E)^2}{(\omega + s\omega_E)^2 - \omega_0^2}. \tag{27}$$

(see [8]). Let us call the region, which is far enough from the resonance region, the *out of resonance region* - **Out**. The equation (27) for this **Out** region becomes

$$\omega^2 = \Omega_0^2 \sum_{s=-\infty}^{s=\infty} J_s^2(\rho_p) \cdot \frac{(s\omega_E)^2}{(s\omega_E)^2 - \omega_0^2} = \omega_0^2 \left(1 - \Phi_x(\rho_p)\right), \tag{28}$$

where $x = \omega_0/\omega_E$, and

$$\Phi_x(\rho_p) = \frac{\pi x}{\sin x} \cdot J_x(\rho_p) \cdot J_{-x}(\rho_p). \tag{29}$$

In (25) to (29) $J(...)$ are Bessel functions. Equation (28) was used here for numerical calculations of ω/Ω_0 and γ/Ω_0 of the oscillations ω, and growth rates γ of these waves when ω^2 becomes negative. By the converse case, namely when

$$\left((\omega + s\omega_E)^2 - \Omega_0^2\right) \ll \omega_0^2,$$

let us call it *the resonance region* - **Res**, the solution of (27) brings to the two following formulas which estimate the oscillations ω and the growth rates γ. Namely for $s = 1$, when $\omega_0/\omega_E \leq 1$,

$$\frac{\omega}{\Omega_0}, \frac{\gamma}{\Omega_0} = \frac{1}{4}\sqrt{\frac{M_{eff}}{m}} \cdot \left\{ \pm(x^2-1)^2 + \left(32 \cdot \frac{M_{eff}}{m} \cdot J_1^2(\rho_p) \cdot |(x^2-1)|\right)^{1/2} \right\}^{1/2}, \tag{30}$$

and for $\omega_0/\omega_E \geq 1$,

$$\frac{\omega}{\Omega_0}, \frac{\gamma}{\Omega_0} = \frac{1}{4}\sqrt{\frac{M_{eff}}{m}} \cdot \left\{ \pm(x^2-1)^2 + \left((x^2-1)^4 + 32 \cdot \frac{M_{eff}}{m} \cdot J_1^2(\rho_p) \cdot |(x^2-1)|\right)^{1/2} \right\}^{1/2}, \tag{31}$$

where M_{eff} is the effective mass of the ions of the plasma and the signs $< \pm >$ in the $\{...\}$ brackets were used by calculation of ω/Ω_0 and γ/Ω_0. Certainly, the frequency region $|\frac{\omega_0}{\omega_E} - 1|$ of applicability of the **Out** and **Res** formulas are not known precisely. Approximately, they might be estimated by the crossing of the **Out** and **Res** branches which are seen on Fig.5 (see below).

Results of numerical calculations by equations (28) of the dependencies ω/Ω_0 and γ/ω_0 in the **Out** region, and by equations (30), (31) in the **Res** region for different values of ρ_p are given on Figs. 3 and 4. The values of the growth rates in the resonance region are specially selected in Table III, and in details they are given for the **Out** resonance region in Table IV. It is seen that for all of the values of ρ_p used here, the maxima of the growth rates γ are comparable with the ion Langmuir frequency. Both dependencies are also presented for the second harmonic, $s = 2$ on Fig.5 for $\rho_p = 1$. The intersection regions of the **Res** and of the **Out** dependencies give a rough presentation of the values (ω_0/ω_E) of applicability of the **Out** and **Res** formulas (28), (29) and (30, 31). They are equal to

$$\left(\frac{\omega_0}{\omega_E}\right)_{Res} \sim (0.9 - 1.1), \quad \left(\frac{\omega_0}{\omega_E}\right)_{Out} \sim (1.1 - 1.8). \tag{32}$$

It was very important to evaluate even roughly the amplitudes E_p of the electric field which may generate the resonance oscillations. For this purpose we used the asymptotic solution of the dispersion equation in the kinetic approximation for an isotropic plasma. If $\omega_0/\omega_E < 1$, the threshold value of the amplitude of the electric field $E_{p,thresh}$, which is necessary for excitation

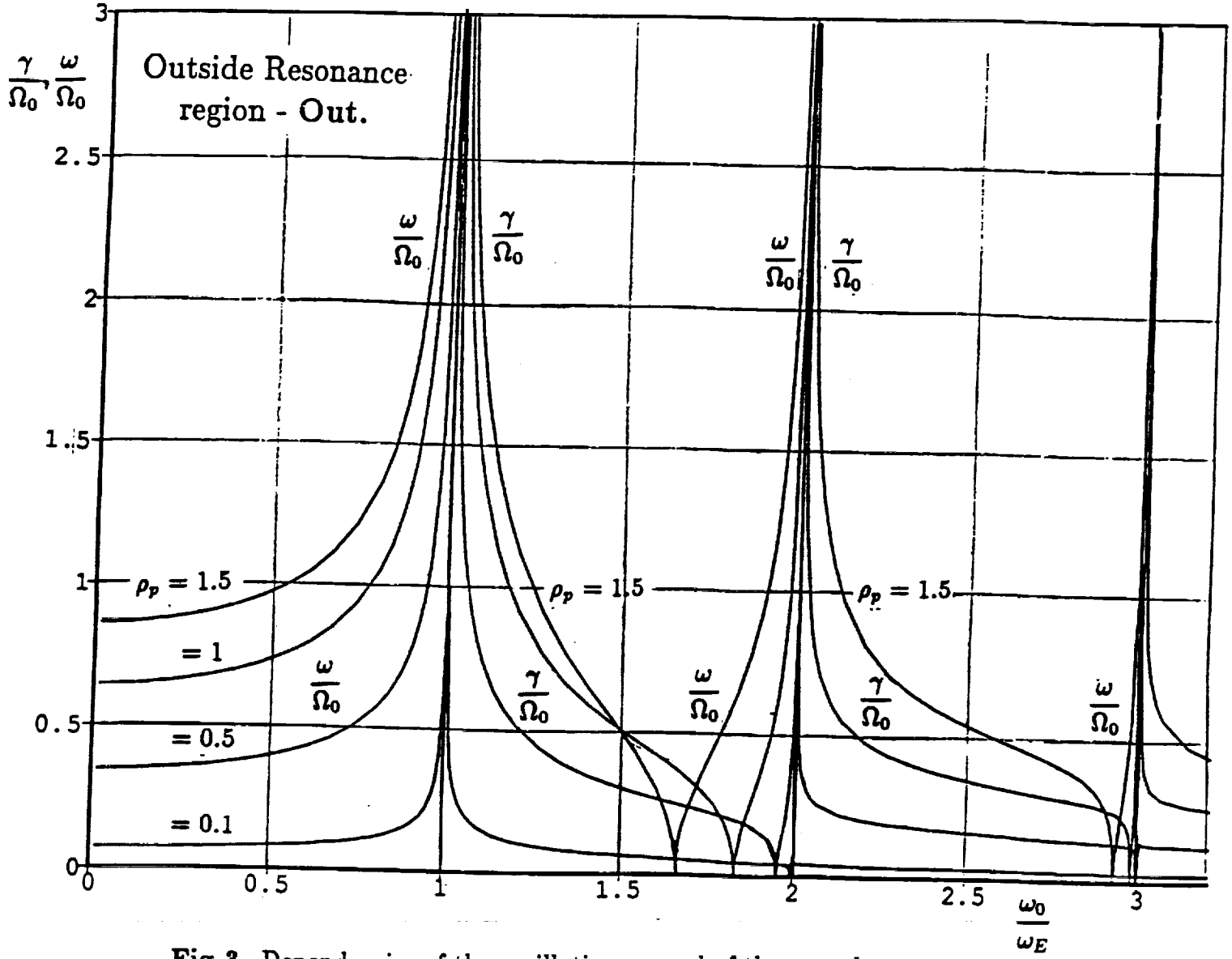

Fig 3. Dependencies of the oscillations ω and of the growth rates γ, $\rho_p \sim E_p/\omega_E^2$, ω_0 is the Langmuir frequency, ω_E is the frequency of the electric field.

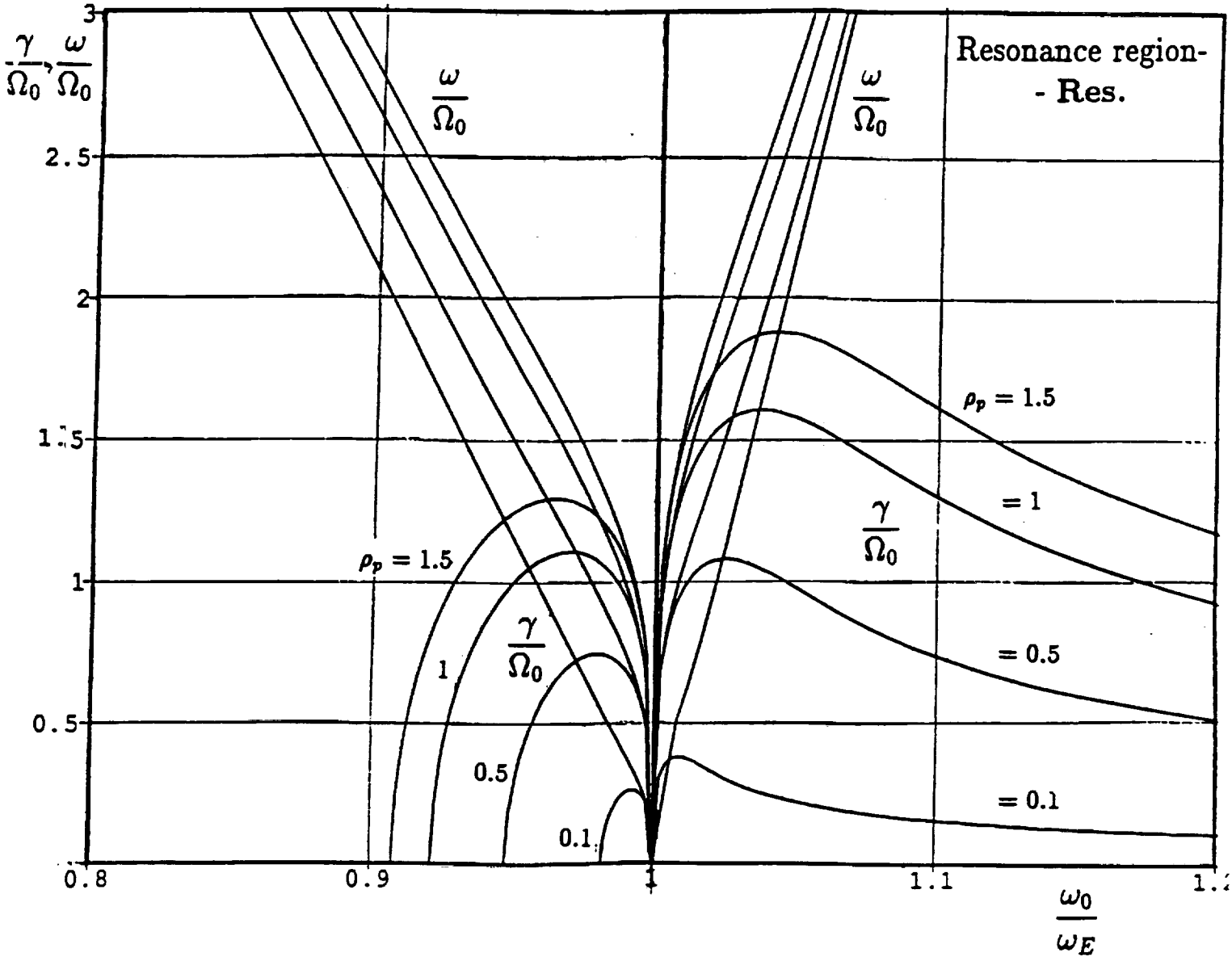

Fig 4. The same as on Fig.3.

Table III. Resonance regions - (Res.)

$$Y = \frac{\gamma}{\Omega_0} = (\alpha_1/4)\cdot\left(\frac{M}{m}\right)^{1/2}\cdot\left(-(x^2-1)^2 + \left(\left(\alpha_2(x^2-1)^4\right) + J_1^2(\rho_p)\cdot\frac{m}{M}\cdot|(x^2-1)|\right)^{1/2}\right)^{1/2}$$

$$x <,= 1: \quad \alpha_1 = 1, \quad \alpha_2 = 0; \quad x >,= 1: \quad \alpha_1 = \sqrt{2}, \quad \alpha_2 = 1$$

$x = \frac{\omega_0}{\omega_E}$	$\rho_p = 1.5$	**1.0**	**0.5**	**0.1**	Δx_{Res}
0.908	0.03	-	-	-	-
0.920	0.80	0.04	-	-	-
0.935	1.09	0.80	-	-	-
0.945	1.20	0.93	0.04	-	-
0.954	1.26	1.02	0.40	-	-
max1:0.9632	1.291	1.08	0.63	-	−0.037
0.9690	-	max1:1.105	0.69	-	−0.031
0.977	-	1.09	-	-	-
0.9794	-	-	max1:0.7423	-	−0.021
0.982	-	-	-	0.009	-
0.984	-	-	-	0.14	-
0.986	-	-	-	0.18	-
0.991	-	-	-	0.25	-
0.9929	-	-	-	max1:0.262	−0.007
1.00	0	0	0	0	-
1.002	-	-	-	0.30	-
1.005	-	-	0.851	0.36	-
1.0088	-	-	-	max2:0.376	+0.009
1.009	1.49	1.31	0.980	0.37	-
1.015	1.66	1.47	1.046	0.35	-
1.026	1.80	-	max2:1.080	0.29	+0.026
1.039	-	max2:1.607	1.065	0.24	+0.039
max2:1.046	1.882	1.56	1.01	0.22	+0.046
1.10	1.161	1.25	0.70	0.15	-
1.15	1.37	1.01	0.60	0.12	-
1.20	1.17	0.94	0.52	0.11	-

Table IV. Resonance outside regions - (Out.)

$$Y = \frac{\omega}{\Omega_0} = \left(1 - \frac{\pi x}{\sin \pi x} \cdot J_x(\rho_p) \cdot J_{-x}(\rho_p)\right)^{1/2}, \quad \rho_p = \frac{e}{m} \cdot \frac{E_p}{\omega_E^2} \cdot \frac{2\pi}{\lambda} = 2\pi \cdot \frac{r_E}{\lambda}$$

$x = \frac{\omega_0}{\omega_E}$	$\rho_p = 0.1$	0.5	1.0	1.5	x	$\rho_p = 0.1$	0.5	1.0	1.5
-	ω/Ω_0	ω/Ω_0	ω/Ω_0	ω/Ω_0	-	γ/Ω_0	ω/Ω_0	ω/Ω_0	ω/Ω_0
0.2	0.072	0.352	0.656	0.874	1.96	0.409	0.077	0.729	1.586
0.3	0.074	0.362	0.673	0.896	1.97	0.403	0.149	0.868	1.848
0.4	0.077	0.376	0.699	0.928	1 99	0.370	0.385	1.587	3.256
0.5	0.081	0.398	0.738	0.976	1.999	0.032	-	-	-
0.6	0.088	0.430	0.797	1.048	-	ω/Ω_0	ω/Ω_0	ω/Ω_0	ω/Ω_0
0.7	0.099	0.482	0.889	1.162	1.999	0.038	1.354	5.127	10.371
0.8	0.118	0.573	1.052	1.366	1.9999	0.172	4.324	-	-
0.85	0.134	0.652	1.195	1.544	2.00	109	26.78	10055	20310
-	-	-	-	-	-	$\to \infty$	$\to \infty$	$\to \infty$	$\to \infty$
0.9	0.162	0.787	1.440	1.850	-	γ/Ω_0	γ/Ω_0	γ/Ω_0	γ/Ω_0
0.95	0.226	1.098	2.002	2.556	2.01	0.044	0.475	1.661	3.307
0.98	0,.54	1.722	3.133	3.984	2.10	0.038	0.229	0.608	1.104
0.99	0.501	2.420	4.416	5.607	2.70	0.028	0.144	0.299	0.436
-	-	-	-	-	2.90	0.026	0.131	0.253	0.260
-	γ/Ω_0	γ/Ω_0	γ/Ω_0	γ/Ω_0	2.93	0.0257	0.130	0.240	0.120
1.00	4370	21201	38510	48826	2.935	-	-	-	0.034
-	$\to \infty$	$\to \infty$	$\to \infty$	$\to \infty$	-	-	-	-	-
1.01	0.498	2.410	4.385	5.551	-	γ/Ω_0	γ/Ω_0	γ/Ω_0	ω/Ω_0
1.02	0.351	1.703	3.090	3.906	2.938	-	-	-	0.088
1.05	0.221	1.070	1.934	2.432	2.94	0.0255	0.129	0.232	0.119
1.10	0.154	0.746	1.343	1.673	2.96	0.0254	0.127	0.208	0.332
1.20	0.106	0.514	0.915	1.112	2.98	0.0252	0.124	0.114	0.627
1.30	0.084	0.408	0.717	0.840	0.2983	-	-	0.053	0.701
1.50	0.063	0.299	0.498	0.491	-	γ/Ω_0	γ/Ω_0	ω/Ω_0	ω/Ω_0
1.55	0.060	0.281	0.457	0.405	2.985	-	-	0.079	-
1.60	0.059	0.278	0.417	0.298	2.99	0.0251	0.120	0.212	0.976
1.655	-	-	-	0.072	2.995	0.0251	0.1109	-	-
-	γ/Ω_0	γ/Ω_0	γ/Ω_0	ω/Ω_0	-	γ/Ω_0	ω/Ω_0	ω/Ω_0	ω/Ω_0
1.66	0.0532	0.247	0.367	0.052	2.999	0.0250	0.059	1.039	3.315
1.67	0.0527	0.244	0.360	0.138	2.9999	0.0249	0.425	-	-
1.70	0.051	0.235	0.329	0.264	2.99999	0.021	-	-	-
1.75	0.49	0.221	0.272	0.412	-	γ/Ω_0	γ/Ω_0	γ/Ω_0	ω/Ω_0
1.80	0.047	0.202	0.181	0.549	3.000	1.52	224	1712	5335
-	-	-	-	-	-	$\to \infty$	$\to \infty$	$\to \infty$	$\to \infty$
1.83	0.046	0.196	0.038	0.639	3.01	0.025	0.134	0.428	1.129
-	γ/Ω_0	γ/Ω_0	ω/Ω_0	ω/Ω_0	3.05	0.0245	0.126	0.298	0.614
1.835	-	-	0.667	-	3.10	0.0241	0.123	0.274	0.508
1.84	0.045	0.192	0.104	0.673	3.12	0.0239	0.0122	0.268	0.487
1.90	0.043	0.160	0.352	0.938	3.15	0.0236	0.121	0.262	0.463
1.95	0.041	0.062	0.631	1.405	3.20	0.0232	0.118	0.253	0.440

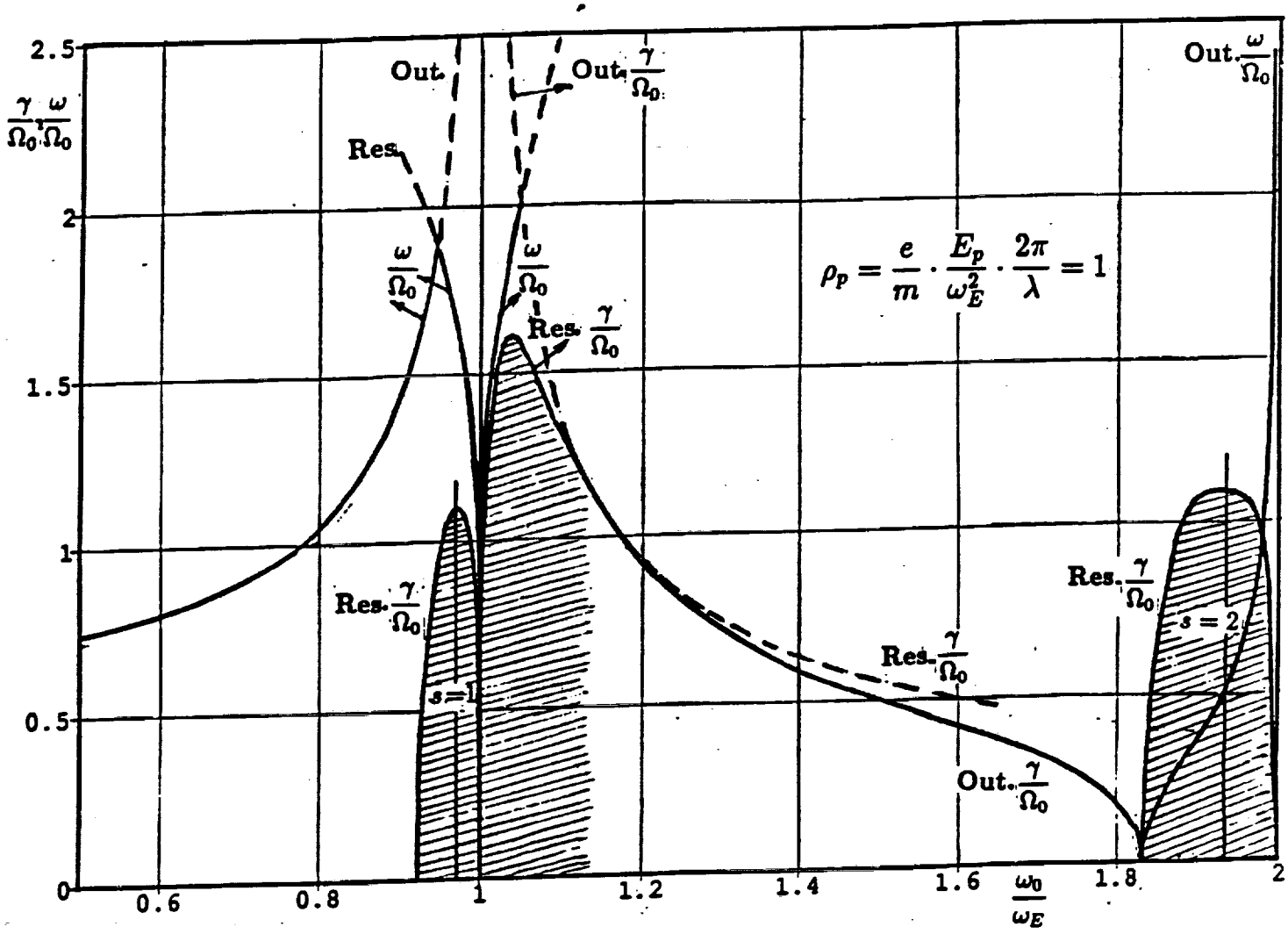

Fig 5. Dependencies of the frequencies ω and growth rates γ in the resonance - **Res** and out-resonance - **Out** regions for $\rho_p = 1$.

of this branch of oscillations, is determined by the formula

$$E^2_{p,thresh} = \frac{4\nu_{ei}}{\omega_0}(4\pi N\kappa T_e + 4\pi N\kappa T_i) = \frac{32\nu_{ei}}{\omega_0}\cdot N\kappa T_{ei}, \qquad (33)$$

and the threshold amplitude r_E of the electron oscillations (see (4)) is determined by

$$r^2_{E,thresh} = \frac{E^2_{p,thresh}(D_e^2 + D_i^2)}{8\pi N\kappa T_e} \qquad (34)$$

In the ionosphere the values of $E_{p,thresh}$ and $r_{E,thresh}$ are equal to:

$Z,\ km$	$E^2_{thresh}\ CGSE,\ E\ V/m$	$r^2_{E,thresh}\ cm^2,\ r_E\ cm$
200	$3.47\cdot 10^{-10},\ 0.56$	$1.51\cdot 10^{-5},\ 3.9$
300	$1.48\cdot 10^{-9},\ 1.15$	$1.09\cdot 10^{-5},\ 3.3$
400	$8.13\cdot 10^{-10},\ 0.86$	$1.42\cdot 10^{-5},\ 3.8$

It is seen that $E_{p,thresh} \sim 1\ V/m$. The used by these calculation values of ν_{ei}, $4\pi N\kappa T_e$, and D_e are given above in the Table of Section II. The region of the applicability of (33) an (34),

$$0 < \omega_E - \sqrt{\omega_0^2 + \Omega_0^2} < \frac{3}{2}\omega_0^2 k^2 D_e^2 \qquad (35)$$

is very narrow and depends on the wave number $k = 2\pi/\lambda$.

When $\omega_E < \sqrt{\omega_0^2 + \Omega_0^2}$ the threshold of the electric field is equal to

$$E_{p,thresh} = 2\cdot(\Delta\cdot 4\pi N_e\kappa T_e + 4\pi N_i\kappa T_i)^{1/2} = 2\sqrt{2}\cdot(\Delta\cdot 4\pi N_e\kappa T_e)^{1/2}, \quad (36)$$

where $\Delta = \left(1 - \omega_E/\sqrt{\omega_0^2 + \Omega_0^2}\right)$. I.e.

$$E_{p,thresh} \sim \sqrt{\frac{\sqrt{\omega_0^2 + \Omega_0^2} - \omega_E}{\sqrt{\omega_0^2 + \Omega_0^2}}} \simeq \sqrt{1 - \frac{\omega_E}{\omega_0}} \tag{37}$$

and it is increases with ω_0/ω_E. In the regions of the maximum value of the growth rates γ/Ω_0 of the VLF resonance oscillations (see Figs. 3, 5, and Table III) the values of $E_{p,thresh}$ are equal to:

Z, km	$E^2_{p,thresh}$ $CGSE$	$E_{p,thresh}$ V/m
200	$5.46 \cdot 10^4$	16.38
300	$1.27 \cdot 10^{-3}$	38.1
400	$1.27 \cdot 10^{-3}$	38.1

They are much larger than the values estimated by (33), and smaller than the critical values of $E_{p,0}$ given in the table of Section II (see (3)).

Thus, the amplitude of the electrical field which can excite the parametric resonance branches $\omega_{1\ to\ 4}$, analyzed in Section III-1, and the VLF resonance oscillations, considered in this section, are changing in different conditions from a fraction of 1 V/m to $(16 - 40)$ V/m, and may be equal to some 10's and even more Volts per meter.

The maximum growth rates of these oscillations described by (33) and

(34) are the following;

$$\frac{\omega_0}{\omega_E} < 1, \quad \left(\frac{\gamma}{\Omega_0}\right)_{max} = \frac{M}{m} \cdot \frac{(r_E^2 - r_{E,thresh})}{r_{D_e}^2 + r_{D_i}^2} \simeq \frac{M}{m} \cdot \frac{r_E^2}{2r_{D_e}^2}, \tag{38}$$

where the amplitude of the oscillations of the electrons is:

$$r_E = \frac{e}{m} \cdot \frac{E_{p,thresh}}{\omega_E^2}. \tag{39}$$

When $\omega_0/\omega_E > 1$, than

$$\left(\frac{\gamma}{\Omega_0}\right)_{max} = \frac{\omega_0}{\Omega_0} \left(\frac{J_1^2(\rho_p)}{2} \cdot \frac{\Omega_0^2}{\omega_0^2}\right)^{1/3}. \tag{40}$$

In the ionosphere the values of $(\gamma/\Omega_0)_{max}$ are the following:

Z, km	r_E^2, cm^2	$r_{E,thresh}^2$, cm^2	$(\gamma/\Omega_0)_{max}$				
			$\omega_0/\omega_E < 1$	$\omega_0/\omega_E > 1$			
				$\rho_p = 1.5$	$\rho_p = 1.0$	$\rho_p = 0.5$	$\rho_p = 0.1$
200	$6.14 \cdot 10^{-3}$	$1.51 \cdot 10^{-5}$	0.34	2.85	2.43	1.64	0.56
300	$3.514 \cdot 10^{-3}$	$1.05 \cdot 10^{-5}$	0.61	2.56	2.18	1.46	0.50
400	$3.151 \cdot 10^{-3}$	$1.42 \cdot 10^{-5}$	0.20	2.27	1.93	1.29	0.44

By calculating $(\gamma/\Omega_0)_{max}$ we used the table given in Section II. It is seen that the growth rates γ_{max} are rather large, and are comparable with the ion Langmuir frequency Ω_0. I.e. the VLF parametric resonances in the ionosphere are phenomena of great *vitality*.

Let us note here that the formula (40) of $(\gamma/\Omega_0)_{max}$ is of pure cold plasma approximation origin. The values of the growth rates, given in the table are a

little smaller than on Fig.3 because they were calculated by using the mass of protons (see Section II). Vice-versa, when $\omega_0/\Omega_E < 1$, they are smaller than the values given in Fig.3. However, the data given here are namely the results of the more correct kinetic approximation, which brings to the formula (38).

b. Anisotropic plasma ($\vec{B} \neq 0$). When the frequency of the electric field $s\omega_E$, $s = 1, 2, ..$ is not much larger than the hybrid resonance frequencies $\omega_3(\Theta)$, $\omega_4(\Theta)$, and $\cos\Theta \gg m/M$, the spectrum of this low frequency band $\omega \ll \omega_E$ may be described by the equation

$$\omega_{\pm}^2 = \frac{\left[\Omega_B^2 + \Omega_0^2 \cdot \Phi(\omega_E, \vec{k})\right]}{2} \pm \pm \frac{\sqrt{\left[\Omega_B^2 + \Omega_0^2 \cdot \Phi(\omega_E, \vec{k})\right]^2 - 4\Omega_B^2\Omega_0^2\Phi(\omega_E, \vec{k})\cos^2\Theta}}{2}, \tag{41}$$

where

$$\Phi(\omega_E, \vec{k}) = \sum_{s=-\infty}^{s=\infty} J_s^2(\rho_{pB}) \cdot \frac{s^2\omega_E^2(s^2\omega_E^2 - \omega_B^2)}{(s^2\omega_E^2 - \omega_3^2)(s^2\omega_E^2 - \omega_4^2)} \tag{42}$$

and $\omega_3(\Theta)$ and $\omega_4(\Theta)$ are estimated by (17). Equation (42) is identically equal to

$$\Phi(\omega_E, \vec{k}) = 1 + \frac{\omega_0^2}{\omega_4^2}\left[\Phi_{x_1}(\rho_{pB}) - \Phi_{x_2}(\rho_{pB})\right] - \Phi_{x_2}(\rho_{pB}), \tag{43}$$

(see [8]), where

$$\Phi_{x_{1,2}}(\rho_{pB}) = \frac{\pi x_{1,2}}{\sin \pi x_{1,2}} \cdot J_{x_{1,2}}(\rho_{pB}) \cdot J_{-x_{1,2}}(\rho_{pB}), \tag{44}$$

and $x_1 = \omega_3(\Theta)/\omega_E$, $x_2 = \omega_4(\Theta)/\omega_E$.

Under the influence of the magnetic field $\overline{B}$ the characteristic parameter of the plasma (see (4)) becomes equal to

$$(\rho_{pB})^2 = \left(\frac{2\pi}{\lambda} \cdot \frac{eE_p}{m\omega_E^2}\right)^2 \cdot k(\chi, \varphi, \Theta), \tag{45}$$

where

$$k(\chi, \varphi, \Theta) = \left[\cos\chi\cos\Theta + \frac{\omega_E^2 \sin\chi \sin\Theta\cos\varphi}{(\omega_E^2 - \omega_B^2)}\right]^2 + \frac{\omega_E^2\omega_B^2(\sin\chi\sin\Theta\sin\varphi)^2}{(\omega_E^2 - \omega_B^2)^2}, \tag{46}$$

and Θ is the angle between the magnetic field $\vec{B}$ and wave vector $\vec{k}$, χ is the angle between $\vec{B}$ and the electric field $\vec{E}$, and φ is the angle between the surfaces $(\vec{k}, \vec{B})$ and $(\vec{E}_p, \vec{B})$.

From (41) and (42) it is seen that when $s\omega_3 < \omega_3(\Theta)$ and $\omega_4(\Theta)$, $\Phi(\omega_E, \vec{k})$ and the roots of (41) become negative, namely $\omega_3^2(\Theta)$ and $\omega_4^2(\Theta) < 0$. I.e. instabilities arise in the magnetoplasma and, particularly, the interested us here oscillations of the hybrid band $\omega_3(\Theta)$ grow up. Their growth rates are maximal when $\rho_B \simeq 1$ and become close to the roots of hybrid branch ω_3^2 (see (41)). Namely, when $\omega^2 \gg \Omega_B^2$

$$\omega_\pm^2 = \frac{s\omega_E^2}{8} \cdot \left|\frac{4\Omega_0^2(s^2\omega_E^2 - \Omega_B^2)J_n^2(\rho_{pB})}{s^2\omega_E^2(2s^2\omega_E^2 - \omega_0^2 - \omega_B^2)}\right|^{2/3} \cdot \alpha_\pm, \tag{47}$$

where $\alpha_\pm$ is a numerical coefficient $\sim (1\ to\ 2)$ (see [8]).

It is important to note here that because of the dependence of the hybrid resonance frequency on the angle Θ, the width of the resonance region in a magnetoplasma is very much broader than in the width of the resonance regions in the ionosphere (isotropic plasma) calculated above. This

circumstance facilitates the discovery of these resonances in the ionosphere by experiments in Situ on satellites.

In the threshold region of the instabilities in the low frequency band $|\omega + i\gamma| \ll \omega_E \sim \omega_3(\Theta)$, when $\Delta\omega_3 = (\omega_E - \omega_3) < 0$, the threshold value of the amplitude of the electric field $E_{p,thresh}$, which is necessary for excitation of this branch of oscillations, is equal to

$$E^2_{p,thresh} = \frac{32\nu_{ei}\omega_E^3}{\omega_0^4} \cdot N\kappa T_{ei} \cdot \left[1 + 2 \cdot \frac{1 - \frac{\omega_0^2}{\omega_E^2}}{1 - \frac{\omega_B^2}{\omega_0^2}}\right], \qquad (48)$$

and the maximal growth rate of these oscillations

$$\gamma_{max} = \frac{\nu_{ei}}{2}\left(\frac{E_p^2}{E^2_{p,thresh}} - 1\right)\left(1 + \frac{\omega_E^2\omega_B^2 \sin^2\Theta}{(\omega_E^2 - \omega_B^2)\cos^2\Theta + \omega_E^4 \sin^2\Theta}\right), \qquad (49)$$

(see the formulae (33) to (38) given above).

Summary

In this report results of numerical theoretical calculations of e.m. oscillations and waves produced in the ionosphere under the influence of the electric field $\vec{E} = \vec{E}_p \cos\omega_E t$ are presented. They are chiefly done for the VLF - $(\Omega_B < \omega \to \Omega_0)$ and ELF - $(0 < \omega < \Omega_B)$ frequency bands, where the parametric activity of the electric field is especially strong (Ω_B and Ω_0 are the gyro- and Langmuir frequencies of the ions).

The resonance branch of *pure electric field origin* $\omega_2(\Theta) = (\Omega_p \ to \ 0$ is of a special interest. The frequency $\Omega_p = \Omega_0 (1 - J_0^2(\rho_p))$ is changing, depending on the amplitude E_p and frequency ω_E of the electric field, from Ω_0 to zero. I.e. parametric longitudinal ELF Alfven waves can be generated in the ionosphere. Another important result is the found dependence *close to the cosine* of the ELF resonance branch $\omega_1(\Theta) = (\Omega_B \rightarrow 0)$. This is in a *strong contrast* to the angle dependence of $\omega_1(\Theta)$, when the electric field is absent. Therefore, this effect may be an indicator of the existence of the electric field in the ionosphere. The necessary amplitudes E_p of the electric field to produce the effects discussed here are changing in different cases between about 1 V/m and some 10's of Volts per meter, and more.

To discover and to investigate these effects by satellite experiments will be an important contribution to the ionosphere knowledge and to plasma physics.

Acknowledgement: I am very grateful to Svetlana Alpert for the exceptionally helpful and laborious computer calculations.

References

1. V.P. Silin, 1964, Non-linear high-frequency conductivity of a plasma, Journ. Exp. Theor. Phys. (JETPh) **47**, 2254 (in Russian).

2. Yu.M. Aliev & V.P. Silin, 1965, Theory of oscillation of a plasma under the influence of a high-frequency electric field, JETPh, **48**, 501, (in

Russian).

3. V.P. Silin, 1966, Kinetic instability of a plasma under the influence of a high-frequency electric field, JETPh, **51**, 1842 (in Russian).

4. D.F.D. Du-Bois & M.V. Goldman, 1965, Radiation-induced instability of electron-plasma oscillations, Phys. Rev. Lett. **14**, 544.

5. D.F.D. Du-Bois & M.V. Goldman, 1967, Parametrically excited plasma fluctuations, Phys. Rev. **164**, 207.

6. Kyoji Nishikawa, 1967, Instability of a weakly ionized plasma induced by an alternating electric field, Progr. Theor. Phys., **37**, 769.

7. Kyoji Nishikawa, 1968, Parametric excision of coupled waves, II Parametric plasmon- photon interaction, J. Phys. Soc. Japan, **24**, 1152.

8. V.P. Silin, 1973, Parametric action of powerful radiation on a plasma, Publishing House Nauka, Moscow.

9. Ya.L. Alpert, 1983, Near-Earth and interplanetary plasma, Cambridge University Press, v. I and II, 1990 - the second edition.

Investigation B

BICEPS Ionospheric Measurements, and their Correlation with Broadband Waveform Degradation in Satellite Communications at Microwave Frequencies

by
Mario D. Grossi

Contents

I. INTRODUCTION

The ionospheric measurements of the BICEPS observation plan have a scientific relevance in themselves, in terms of improved knowledge that through them will be gained on the ionosphere and the magnetosphere.

Additionally, these measurements have an important application potential to communications, could the BICEPS measurements be correlated (and this is a distinct possibility) with the degradation of the communication waveform (due to ionospheric effects) experienced by satellite microwave links. These microwave paths extend from geosynchronous height to ground and do cross (at the same time that the BICEPS measurements are made) the volume of the ionosphere where BICEPS operates.

With the ever-increasing bandwidth requirements in satellite-to-ground microwave communications, and with the continuous progress in communications equipment technology (that makes gigahertz-bandwiths feasible),the frequency-spread and time-spread characteristics of transionospheric propagation paths are fast becoming the limiting factors in achievable communications performance, in terms of data rate and error rate.

An ionospheric science mission such as BICEPS, if coordinated with existing broad-band microwave links from synchronous heights to ground, would make a vital contribution to the understanding of the limitations imposed by the ionosphere on microwave link performance. Ionospheric effects would be measured in real time , for comparison with their influence on the waveforms transmitted at microwave from synchronous heights to ground (with their propagation paths intersecting the ionospheric regions where BICEPS performs its measurements).

Once that causes and effects are well understood , it will be possible to design a signal processor, to be added to the ground terminals of the satellite microwave link, with the goal of reducing as much as feasible the limitations imposed by the ionosphere on link's performance.

The channel is time spread and frequency spread , and a full correction would require a "phase conjugation" approach, never tried at microwave.However, it might be possible to correct for gross features, such as the waveform degradation experienced by a short pulse. An inverse filtering approach would be quite effective in correcting for this degradation,we would expect.

II - BICEPS Ionospheric Measurements

The basic experimental arrangement for INVESTIGATION B is a multifrequency phase-coherent link established between the two terminal of the pair of BICEPS satellites. BICEPS (Bistatic Canadian Experiment on Plasmas in Space) could use two separate free-flyers called WISPRS (Wave in Space Plasma Research Satellite) or the tethered pair BOLAS (Bistatic Observations using Low-Altitude Satellites). For WISPRS, separation distance is from a few meters to several tens kilometers, while for BOLAS is, at most, 1 kilometer (the length of the tether). However, the tether will be cut at the end of the initial series of measurements, and the two satellites will drift apart freely up to large distances, making the configuration as suitable to general-purpose bistatic measurements as WISPRS.

The scientific objective of INVESTIGATION B is to detect and characterize electron density perturbations in the ionosphere, such as large-scale to small-scale disturbances, T.I. D.s, irregularities producing scintillation, spread-F phenomena, etc. The frequency band of the bistatic sounding will be 0.1 MHz to 20 MHz.

Specific phenomena to be obserbed are the following.

Travelling Ionospheric Disturbances and Atmospheric Gravity Waves Atmospheric gravity waves (AGWs) are an important mechanism by which energy and momentum are transported from one region of the atmosphere to another. Their ionospheric manifestations are called Travelling Ionospheric Disturbances (TIDs) [e.g Hines, 1974]. There are many sources of AGWs: auroral, meteorological, stratospheric and mesospheric heating, and geological. In the thermosphere the energy carried by these waves can be comparable to the input from solar EUV [e.g. Ching and Chiu, 1973]. AGWs may grow non-linearly, generating smaller scale structures in ionization and turbulence in the atmosphere [e.g. Costa and Kelley, 1978].

One of the most important sources of thermospheric TIDs is Joule heating by auroral precipitation, generating wavelengths from tens of centimetres (acoustic waves) to thousands of kilometres (gravity waves). These waves propagate to mid-latitudes and are believed to be a cause of mid-latitude spread F [e.g. Bowman, 1981]. The direction of arrival measurements provided by the Doppler capability [Dyson, 1978] of the BICEPS receiver will provide a new ability to map details of TID structure from satellites and relate them to sources and spread F. AGWs dissipate as they propagate to high altitudes and their interaction with the ionosphere causes the effects of TIDs to be greatest near the F-layer peak. TIDs generally have horizontal wavelengths greater than 100 km but structure with smaller wavelengths occurs in association with spread F. Consequently the BICEPS TID study will be capable of observing horizontal structures spanning tens to thousands of kilometres.

The specific aims of BICEPS TID study will be to:

- Determine TID wave characteristics near the F-layer peak (wavenumber, direction of travel, frequency and amplitude);
- Locate sources of the waves;
- Infer the energy and momentum transferred by TIDs and the AGWs driving them;
- Determine the occurrence and structure of smaller-scale disturbances generated by TIDs.

An important aspect of achieving these aims will be simultaneous observations by ground-based ionospheric radars.

Mid-latitude spread F Generally mid-latitude spread F is not as severe as that occurring at low and high latitudes and there is still no accepted theory explaining its cause. Many measurements indicate that the structures responsible are "ripples" with horizontal scale-sizes of tens of kilometres [e.g. Bowman, 1960; Scali, 1989]. However other measurements indicate smaller irregularities may sometimes be significant [Bowman et al, 1988; Dyson and Roberts, 1989]. The situation is further complicated by occurrences of very severe spread F but these are clearly associated with irregularities moving equatorward from higher latitudes [Scali and Dyson, 1992]. BICEPS will offer a unique opportunity to study mid-latitude spread F. The BICEPS sounder will detect spread F and the measurement of the direction of arrival using the Doppler shift will allow us to distinguish "ripple" structure. The latitude coverage will enable the boundary of high latitude spread F to be determined, as will the analysis of the amplitude statistics [Scali and Dyson, 1992]. The Langmuir probes can be used to determine the irregularity spectrum, crucial information in determining whether plasma instabilities are involved. Observations near perigee are preferred, and co-ordinated ground-based ionospheric radar measurements will be important.

Large-scale structure Complicated large-scale ionospheric structures occur in the transition from typical mid- to typical high latitude conditions. At night the transition is marked by a pronounced trough in electron density and minor troughs can occur as well [Muldrew, 1965]. Total-electron-content (TEC) [Davies, 1969] observations reveal large-scale ionospheric structure and recent measurements over southern Australia show an ionization enhancement in the early evening possibly related to equatorward movement or expansion of high latitude convective circulation [Breed et al., 1992]. In early winter spread F at mid-latitude stations can be primarily due to equatorward movement of high latitude ionospheric structures [Scali and Dyson, 1992].

The BICEPS sounder will be used to study the features of the mid- to high-latitude transition that are not understood. The sounder has the advantage over other measurement techniques of being able to measure both horizontal and height variations in the ionosphere. The Doppler-direction of arrival capability will enable vertical echoes to be distinguished in the presence of spread F, further enhancing the ability to determine large-scale ionospheric structure. Simultaneous measurements with the Langmuir probes will provide measurements of electron temperature, enabling regions of ionospheric heating to be identified. The particle detectors will also identify regions of energy input.

Solar control phenomena A particular experiment that capitalizes on the bistatic configuration is the measurement of the refractive Doppler shifts (using phase-coherent carriers of the HF link) caused not only by well-known large scale features of the ionosphere

(such as the equatorial geomagnetic anomaly), but also by lesser-known features, such as the sharp peak in electron density that occasionally appears at the day-to-night transition, and that may be due to terminator-related shock waves. The latter features were observed in some of the orbits of the Apollo-Soyuz Test Project (ASTP) spacecraft-to-spacecraft ionospheric sounding [Estes and Grossi, 1984].

Figure 1 shows an example of the results of the ASTP space-to-space sounding. The day/night transition and magnetic equator crossings are indicated in the figures. This marking is almost superfluous for the day/night transitions, since the change in electron density is so dramatic. Daytime crossings of the equator are from south to north, and nighttime crossings from north to south.

A prominent feature seen repeatedly in different revolutions is the geomagnetic anomaly or equatorial trough first observed by Appleton [1946] in which the electron-depleted magnetic equator is flanked by crests to the north and south. In addition to the well-known features mentioned above, i.e., day/night ionization differences and the Appleton anomaly, there is another feature that should be noted. In the two consecutive revolutions displayed in Figure 1 there is a sharp peak in electron density just on the day side of the day-to-night transition point. The peak is especially prominent in the second revolution. This phenomenon may be related to the motion of the terminator with respect to the ionosphere. The proposed high-inclination orbit and telemetry facility for BICEPS mean that the solar terminator will be routinely observable once per orbit on a significant number of occasions throughout the mission.

It has been suggested that a shock wave generated by the supersonic motion of the terminator could be a source of TID, or of other irregularities associated with spread-F phenomena. The condition for supersonic motion to occur is [Cole, 1974]:

$$V_T + V_{aE} > V_s$$

where V_T is the speed of the terminator with respect to the rotating earth coordinate frame, V_{aE} is the wind speed (positive toward the east), and V_s is the speed of sound. The irregularity of the winds and the consequent variability of the wind speed may account for the fact that, on the occasion of the ASTP experiment, the peak was observed only in two revolutions.

TIDs generated by the supersonic motion of the moon's shadow across the earth have been observed. Some authors have also reported evidence for dawn supersonic terminator generation of gravity waves in Langmuir probe data taken by the ESRO 1A satellite. Still, few observations have been performed of terminator-related phenomena. BICEPS observations may help to bring this subject to the deserved attention of theoreticians and experimentalists.

Topside sounders provide the only means of studying simultaneously details of height

and latitudinal variations of the equatorial anomaly. Consequently BICEPS sounder data will be used to test the ability of ionospheric models to predict the anomaly behaviour. Recently methods have been developed to derive neutral winds from ionosonde measurements of the height of the F-layer [Richards, 1991]. While these methods have been applied to mid-latitudes where vertical electrodynamic drift can be ignored, their application to low-latitude BICEPS data would provide measurements of vertical ionospheric drift and its latitudinal variation.

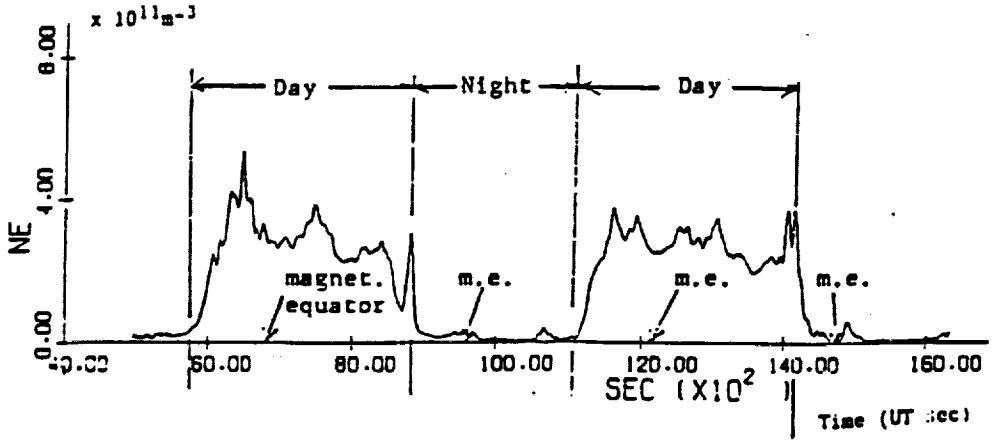

Figure 1

At the Day-to-Night transitions are visible very sharp, strong, localized enhancements of electron density. This is one of the records of electron density measurements obtained by the Apollo-Soyuz Test Project (ASTP), with a phase coherent Doppler link established between the two spacecraft. The electron density is shown as a function of time, with each second corresponding to about 7.8 Km of covered distance.Time is given in UT seconds on July 24, 1975.

III- Broad-band Waveform Degradation due to Ionospheric Effects, in Microwave Communications Links

By moving to higher and higher frequencies, such as to 20 to 30 GHz, it is generally believed that a microwave link in transionospheric paths (typically from geosynchronous height to ground) is not affected in any appreciable way by the ionosphere. We want to show in this Section that this is not the case, and that, by performing simultaneous observations with a microwave link from geosynchronous orbit to ground, and with an orbiting bistatic sounder such as BICEPS, we could collect new evidence on the effect of the ionosphere on the communication performance of the microwave link.

It is known that there are amplitude fluctuation phenomena of a few decibel in links at 20 to 30 GHz from geosynchronous orbit to ground, and it would be of great interest to perform measurements (by BICEPS) of ionospheric irregularities in the microwave propagation path, to explain the observed scintillations. However, even with a totally unperturbed ionosphere, just the columnar content of electrons along the extended propagation path causes a serious degradation of the radiated waveform, when pulse widths are 1 to 10 nanosecond (corresponding respectively to 1 Gigabit/sec and 100 Megabit/sec data rates). These rates are currently either in use or contemplated by advanced communications satellites, such as ACTS (Advanced Communication Technology Satellite).

We have performed an analysis to ascertain the extent of the problem. Here are our findings.

The ionosphere is a dispersive medium (velocity of propagation is a function of frequency, for e.m. waves) and its phase constant $\beta(\omega) = 2\pi/\lambda_{iono}$ has a very simple analytical expression, if we neglect the effect of the geomagnetic field and of collisions (these simplifying assumptions are acceptable at the frequencies of the ACTS links):

$$\beta(\omega) = \frac{2\pi\,\mu}{\lambda_{fs}} = \frac{2\pi f \mu}{c} = \frac{\omega}{c}\mu$$

where : μ = index of refraction = $\sqrt{1 - \frac{\omega_{pe}^2}{\omega^2}}$

λ_{fs} = free space wavelength = $\frac{c}{f}$

c = velocity of light = $3\ 10^8$ m/sec

ω_{pe}^2 = (electron plasma frequency)^2 = $\frac{N e^2}{m \varepsilon_0}$

e = electron charge = $1.602\ 10^{-19}$ Coulomb

m = electron mass = $9.108\ 10^{-31}$ Kg

ε_0 = free space permittivity = $8.85\ 10^{-12}$ F/m

N = ionospheric electron density, el/m^3

We have, therefore :

$$\beta(\omega) = \frac{\omega}{c}\sqrt{1 - \frac{\omega_{pe}^2}{\omega^2}} = \frac{\sqrt{\omega^2 - \omega_{pe}^2}}{c} \qquad [1]$$

Equation [1] can be expanded in a Taylor series about the link's angular frequency ω_o :

$$\beta(\omega) = \beta_o + A(\omega - \omega_o) - B(\omega - \omega_o)^2 + \text{-----}.$$

where $$\beta_o = \beta(\omega_o) = \frac{\sqrt{\omega_o^2 - \omega_{pe}^2}}{c} \cong \frac{\omega_o}{c}$$

$$A = \frac{\omega_o}{c^2 \beta_o}$$

$$B = \frac{1}{2} \frac{\omega_{pe}^2}{c^4 \beta_o^3}$$

Following the treatment by Elliott (1957), as amended by Knop & Cohn (1962), of pulse waveform degradation in a dispersive medium (the case considered by these Authors was a waveguide), we can perform in a simple way an initial estimate of the pulse degradation to be expected in transionospheric paths from geosynchronous height to ground (these are the ACTS paths). First step is the computation of the so-called Elliott parameter a ($a = \frac{4}{T}\sqrt{BL}$), where T is the length of the propagating pulse, B has been defined above, and L is the length of the link (in our case from geosynchronous height to ground). The second step consists of examining the family of curves in Knop & Cohn (1962), that show the various degrees of waveform degradation, for various values of the parameter a , and of selecting the one that matches the value of a determined above. A more precise estimate could be obtained, but it is not done here, by inserting the value of a that we have found, into Equation (1) of Knop & Cohn (1962),that replaces equation (14) of Elliott (1957) that was incorrect. We reproduce in Figure 2 (and in TABLE I) Knop & Cohn's family of curves.

For the case of interest to ACTS, we want to ascertain whether or not transionospheric propagation from geosynchronous height to ground, at 20 -to-30 GHz, causes an appreciable distortion of the ACTS modulation pulses. We take the width of the pulse T to be T = 1-to-10 nanosecond, where the value T=10 nanosec is the equivalent pulsewidth of the 100 Megabit/sec rate, and T= 1 nanosec applies to the case of the forthcoming 1 Gigabit/sec rate. We start by computing :

$$BL = \frac{1}{2}\left(\frac{1}{c^4 \beta_o^3}\right)\left(\frac{e^2}{m \varepsilon_o}\right)\int_0^L N \, dl$$

where $\beta_o \cong \frac{\omega_o}{c} = 418.9 \text{ sec}^{-1}$ (for the frequency of 20 GHz)

$\int_0^L N \, dl$ = total (columnar) electron content of the entire ionosphere, el/m^2 (see Figure 3)

We have therefore that :

$$BL = \frac{1}{2}\left(\frac{1}{81\times10^{32}\times 7.35\times10^{7}}\right)\left(\frac{1.602^{2}\times10^{-38}}{9.108\times10^{-31}\times 8.85\times10^{-12}}\right)\int_{0}^{L} N\,dl$$

$$= 0.267\times10^{-38}\int_{0}^{L} N\,dl\,.$$

From Figure 3, we find that the largest Total Electron Content for Noon-Time (at the equinoxes, and for a high Mean Sun Spot number) is 10^{18} el/m^2. In the same Figure, we read the smallest Content to be $2\ 10^{17}$ el/m^2. Consequently, we have :

$$\begin{cases} \sqrt{BL} = 0.517\ 10^{-10} & \text{for } \int_{0}^{L} N\,dl = 10^{18}\ \text{el/m}^2 \quad (\text{maximum}) \\ \sqrt{BL} = 0.231\ 10^{-10} & \text{for } \int_{0}^{L} N\,dl = 2\ 10^{17}\ \text{el/m}^2 \quad (\text{minimum}) \end{cases}$$

The corresponding values of the parameter $\underline{a}$ are :

$$\underline{a} = \frac{4}{T}\sqrt{BL} = \begin{cases} 0.021 & (\text{max}) \\ 0.009 & (\text{min}) \end{cases} \qquad \text{for T = 10 nanosec}$$

$$\underline{a} = \frac{4}{T}\sqrt{BL} = \begin{cases} 0.21 & (\text{max}) \\ 0.09 & (\text{min}) \end{cases} \qquad \text{for T = 1 nanosec}$$

We can now enter into the family of distorted curves in Knop & Cohn (1962). We see that the case of the 10 nanosecond pulse falls between curve A (the reference curve) and curve B . The waveform distortion is limited, but still measurable. The 1 nanosecond pulse is, on the contrary, heavily distorted (we fall between curve C and curve D), and this would create serious problems in achieving the goal of 1 Gigabit/sec data rate, if left uncorrected. Correction could be sought through the application of inverse filtering.

We conclude that the effect of the ionosphere on the performance of a microwave communications link from geosynchronous orbit to ground is significant and that BICEPS measurements would be very useful, if done along the microwave propagation path, to establish the correlation between ionospheric parameters and link's performance.

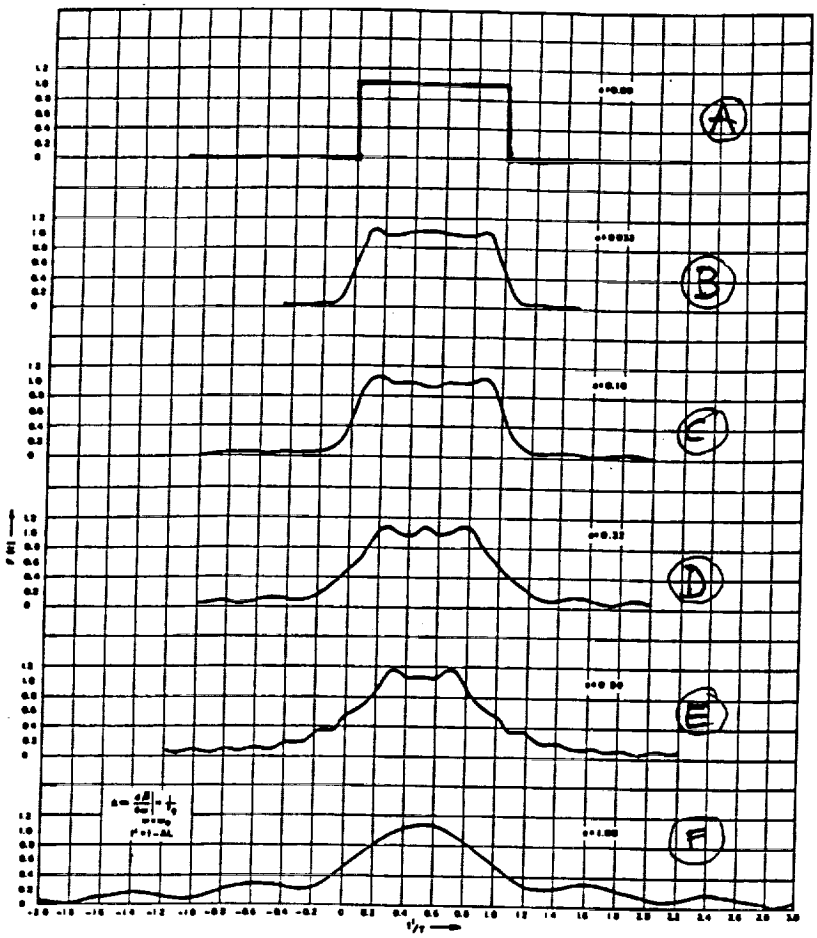

From: Knop & Cohn, 1962

Fig. 2—Degraded waveforms.

TABLE I

TABULATION OF $\sqrt{\frac{X^2 + Y^2}{2}}$

t'/T	$\alpha = 0.00$	$\alpha = 0.032$	$\alpha = 0.10$	$\alpha = 0.32$	$\alpha = 0.50$	$\alpha = 1.00$
0.0	1.00	0.495	0.495	0.523	0.538	0.523
0.1	1.00	1.022	1.020	0.791	0.672	0.691
0.2	1.00	0.973	1.024	1.080	0.887	0.846
0.3	1.00	0.984	0.981	1.044	1.180	0.971
0.4	1.00	1.000	0.992	0.967	1.051	1.051
0.5	1.00	1.016	0.946	1.098	1.045	1.080
0.6	1.00	1.000	0.992	0.967	1.051	1.051
0.7	1.00	0.984	0.981	1.044	1.180	0.971
0.8	1.00	0.973	1.024	1.080	0.887	0.846
0.9	1.00	1.022	1.020	0.741	0.672	0.691
1.0	1.00	0.495	0.495	0.523	0.538	0.523
1.1	0.00	0.045	0.149	0.350	0.326	0.366
1.2	0.00	0.026	0.065	0.209	0.318	0.254
1.3		0.012	0.040	0.111	0.170	0.224
1.4		0.014	0.043	0.107	0.208	0.253
1.5		0.010	0.035	0.118	0.105	0.285
1.6			0.018	0.089	0.152	0.291
1.7			0.017	0.042	0.075	0.266
1.8			0.025	0.050	0.119	0.214
1.9			0.019	0.072	0.061	0.147
2.0			0.007	0.060	0.097	0.082
2.1					0.052	0.064
2.2					0.091	0.103
2.4						0.139
2.4						0.155
2.5						0.148
2.6						0.122
2.7						0.081
2.8						0.038
2.9						0.034
3.0						0.067

Additional Points

t'/T	$\alpha = 0.50$
0.25	1.095
0.35	1.135
0.45	1.035
0.55	1.035
0.65	1.135
0.75	1.095
1.05	0.375
1.15	0.360
1.25	0.206

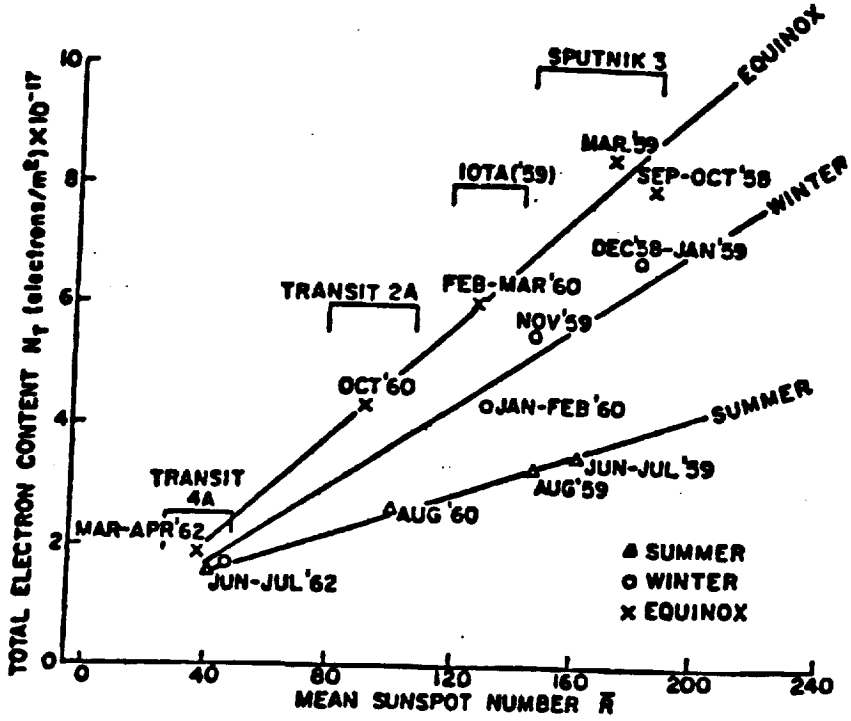

Figure 3

Total electron content of the ionosphere (Noon local time) as a function of Mean Sunspot Number, with season as a parameter (from Bhonsle et al, 1965)

IV- Proposed Experiment with Simultaneous Observations with BICEPS and ACTS Geosynchronous Satellite

A satellite that would be very suitable for the simultaneous measurements to be performed by BICEPS,is the ACTS Advanced Communications Technology Satellite, could BICEPS be launched in orbit in a few years from today, while ACTS is still fully operational.

ACTS was launched to synchronous height by NASA in September 1993 and is expected to have a lifetime of several years. ACTS is a multibeam, Ka-band communications satellite, and is located on the meridian of Denver, Colorado. It uses a 30 GHz uplink, and a 20 GHz down-link. Its bandwidth is nominally 1 GHz. The data rate is at present 100 Gigabit/sec, while consideration is being given to increase it to 1 Gigabit/sec. The multibeam antenna has fixed and hopping spot beams. Several ground stations have been already established in Continental US, but the satellite has also a steerable antenna that can be aimed, for instance, at Hawaii and at Alaska (see Figures 4 and 5). It would be advisable to establish a terminal in Canada, possibly at very high latitudes, close to the Northern edge of the Earth surface that is covered by ACTS. This would be an Experimenter Terminal, that would work in association with the BICEPS mission.

The waveforms that ACTS should transmit for us are : (a) a time-domain short pulse, or equivalent waveform , with the shortest possible risetime (1 nanosecond would be compatible with the stated nominal bandwidth of 1 GHz; however, a few nanosecond would be adequate); (b) a pure CW carrier, 20 GHz to 30 GHz; (c) other waveforms, as required to characterize the microwave channel. These waveforms could be transmitted sequentially and would measure such fundamental channel parameters as time spread (inclusive of multipath), and frequency spread (Doppler shift and spread). Second-order channel functions could also be measured, such as channel correlation functions.

The role of BICEPS would be,fundamentally,to perform measurements that would explain in terms of ionospheric phenomena and structures, the propagation-induced non-idealities, as appearing in the microwave link. The reason is that the propagation paths from ACTS to ground are trans-ionospheric and pass through the volume of the ionosphere where BICEPS performs its measurements. For a fraction of many orbits, BICEPS (either in the BOLAS or the WISPRS configuration)would perform bistatic ionospheric sounding in the volume of interest. In particular, BICEPS would detect and measure E-region and F-region electron density irregularities, Travelling Ionospheric Disturbances, large-scale and small-scale disturbances, spread-F phenomena, terminator-related electron density enhancements, aurora phenomena ,and other time-varying, highly dynamical features of the ionosphere. These features directly affect the microwave link that passes through, and are the cause of its time and frequency spreads. BICEPS would give an unprecedented opportunity to measure simultaneously cause and effects. With this newly acquired knowledge on hand, it would be feasible to design a signal processor that could correct for ionospheric effects and make it possible to utilize to its fullest the broadband that the link's hardware provides (in the case of ACTS, we could prove that 1 GHz bandwidth is becoming fully usable, with the processor, even at the Northern edge of its coverage).

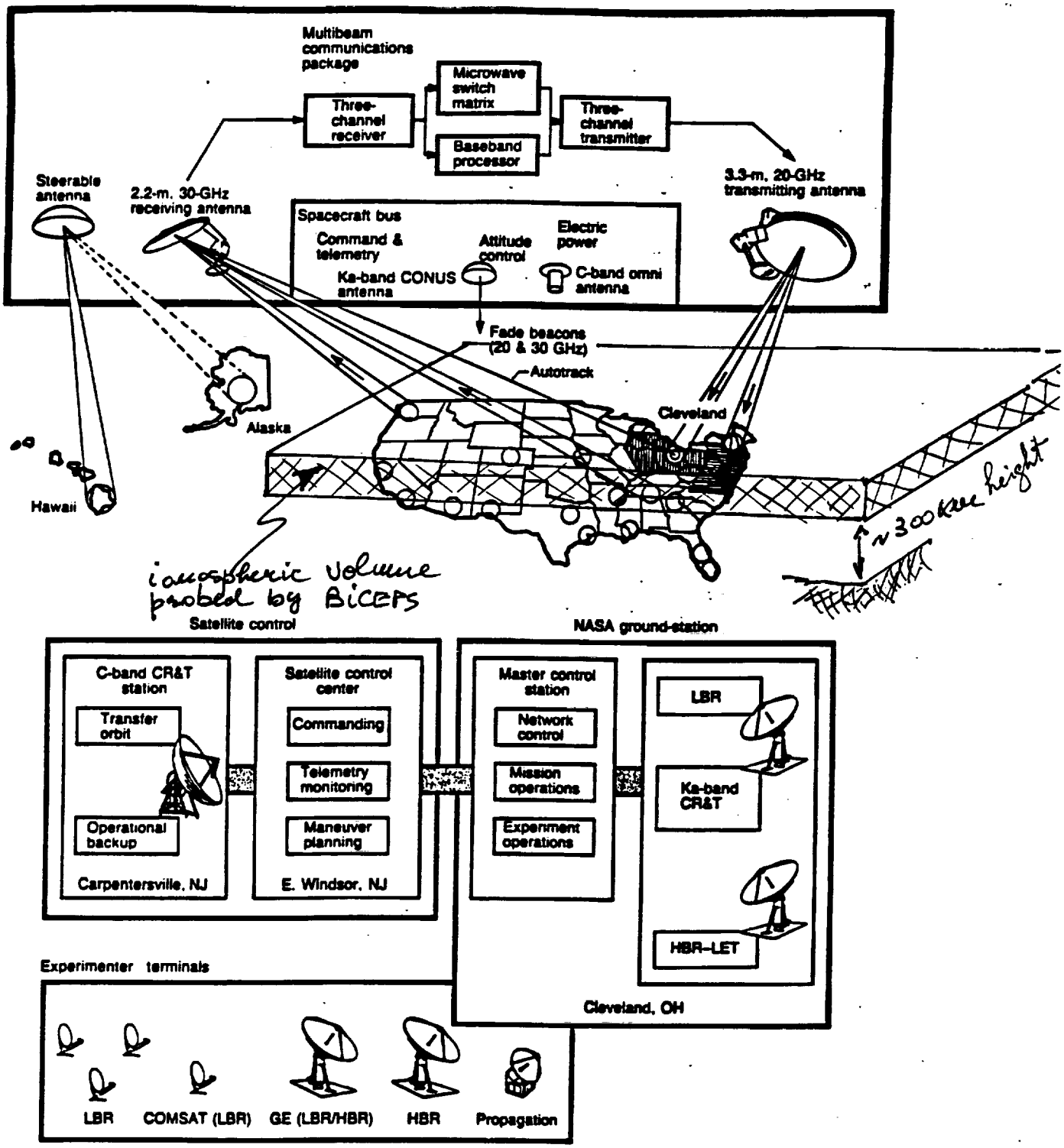

Figure 4
ACTS functions and geometric relationship of ACTS antenna beams and ionospheric volume probed by BICEPS

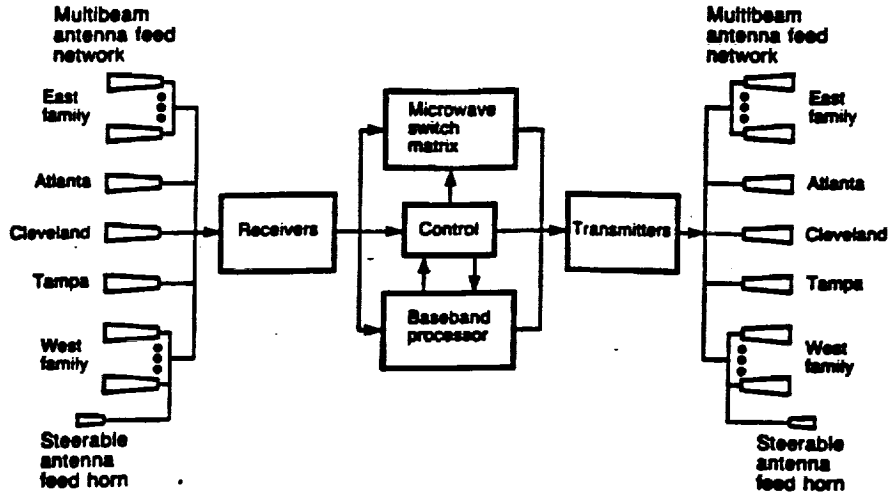

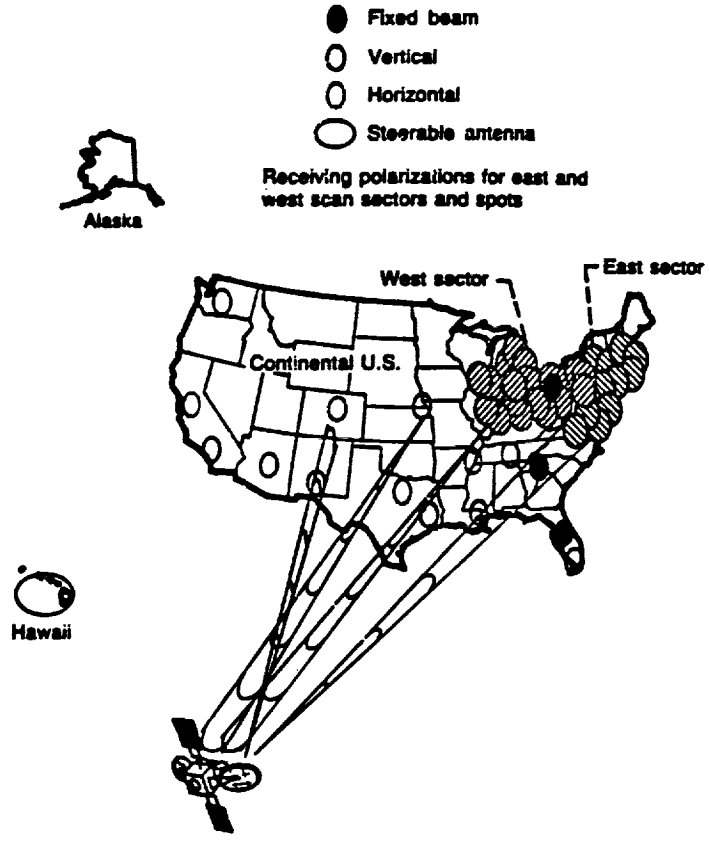

Figure 5
Coverage of ACTS antenna beams and multibeam communications package

V - Bibliographis References

Appleton, E.V., 1946, Nature, 157, 691.

Bowman, G.G., 1960, Planet. Sp. Sci., 2. 133.

Bowman, G.G., 1981, JATP, 43, 65-79.

Bowman, G.G. et al., 1988, JATP, 50, 797.

Breed A.M., et al, 1992, South Pacific STEP Workshop Proceedings, Eds. E.A. Essex and J.D.Whitehead, La Trobe U. Press, Australia, 97-100.

Calvert W. and C.W. Schmid, 1964, JGR, 69, 1839-1852.

Ching B.K. and Y.T. Chin, 1973, Planet.Sp.Sci., 21, 1633-1646.

Cole, K.D., 1974, JATP, 36, 1099.

Costa E. and M.C. Kelley, 1978, JGR, 83, 4359-4364.

Davies, K., 1969, Ionospheric Radio Waves, 460 pp, Blaisdell, Waltham, MA.

Dyson, P.L., 1978, NASA Tech.Memorandum # 79657, GSFC, Greenbelt, MD.

Dyson, P.L., and D.I. Roberts, 1989, JATP, 51, 279-289.

Estes ,R.D. and M.D. Grossi, 1984, Radio Science, 19, 1098-1110.

Hines, C.O., 1974, Geophys. Monograph #18, AGU, Washington, D.C.

Lobb,R.J. and J.E. Titheridge, 1977, JATP, 39, 129-138.

Muldrew, D.B., 1965, JGR, 70, 2635.

Richards, P.G., 1991, JGR, 96, 17839-17846.

Scali J.L., 1989, PhD Thesis, La Trobe U., Australia.

Scali J.L. and P.L. Dyson, 1992, JATP, 54, 265-276.

Elliott, R.S., 1957, IRE Trans. Microwave Th.and Tech., Vol. MTT-5, pp. 254-257,October.

Knop C.M. and G.I. Cohn, 1962, IEEE Trans.Microwave Th. and Tech., pp 445-447, September.

Bhonsle, R.V. et al, 1965, Radio Science, J.of Res. NBS, 69 D, p. 929.